

## Chapter 19

# *The Treatment of Boundary Conditions*

In the preceding chapters, no particular reference was made to the associated boundary conditions, although this is an essential aspect of the practical application of a scheme into a working code.

The reader who has attempted to apply any of the methods described in the previous sections to a flow in a finite domain, for instance a stationary, one-dimensional nozzle flow, is immediately faced with the problem of how to discretize the equations at the boundary points.

Since we deal with hyperbolic propagation-dominated systems, the following essential questions have to be answered:

- (1) How many conditions of physical origin are to be imposed at a given boundary?
- (2) How are the remaining variables to be defined at the boundaries?
- (3) How are these conditions to be formulated and discretized in order to be compatible with the order of accuracy and the stability conditions of the internal scheme?

We will first present an analysis of these questions, and of their answers, for one-dimensional Euler flows.

The outcome of the one-dimensional analysis is actually of direct application to multi-dimensional flows. Indeed, as seen in Section 16.5, the number and type of conditions at a boundary of a multi-dimensional domain are defined by the eigenvalue spectrum of the Jacobians associated with the normal to the boundary. This defines locally quasi-one-dimensional propagation properties. Therefore, we will give a detailed discussion of the one-dimensional boundary treatments for the Euler equations in Section 19.1, while the multi-dimensional aspects will be dealt with in Section 19.2.

Section 19.3 gives a brief mention of far-field boundary conditions, while Section 19.4 discusses the question of the Kutta condition with Euler calculations.

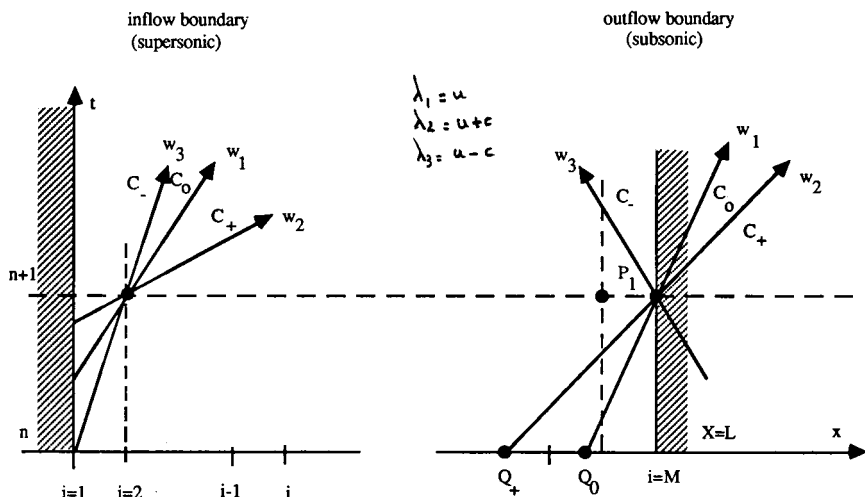


Figure 19.1.1 Boundary conditions for a supersonic inlet and subsonic outlet in a one-dimensional flow

## 19.1 ONE-DIMENSIONAL BOUNDARY TREATMENT FOR EULER EQUATIONS

If a one-dimensional flow problem has to be solved in a range  $0 \leq x \leq L$ , where  $x=0$  is the inflow boundary and  $x=L$  the outflow boundary, the application of any scheme requires the knowledge of the flow variables at the points  $x=0$  and  $x=L$ . We will consider that the space interval  $(0, L)$  is divided into  $(M-1)$  cells of length  $\Delta x$ , ranging from  $i=1$  at  $x=0$  to  $i=M$  at  $x=L$  (Figure 19.1.1).

For instance, writing the explicit Lax-Wendroff scheme at the point next to the inflow boundary,  $i=2$ , leads to

$$U_2^{n+1} - U_2^n = -\frac{\tau}{2}(f_3 - f_1)^n + \frac{\tau^2}{2}[A_{3/2}(f_3 - f_2) - A_{1/2}(f_2 - f_1)]^n \quad (19.1.1)$$

where the right-hand side is taken at time level  $n$ . The values of the dependent variable vector  $U_1$  at point  $x=0$  have to be determined in some way, since one cannot write equation (19.1.1) at  $i=1$  as this would require values of the flow variables at  $i=-1$ , which lies outside the computational domain.

If an explicit scheme is applied, the influence of the boundary values propagate numerically one space step at a time, that is a change in  $U_1$  at time  $n$  will influence  $U_2$  at time  $(n+1)$ ,  $U_3$  at time  $(n+2)$  and so on.

On the other hand, an implicit scheme couples all the points at the same time level and a change in  $U_1$  at time  $n\Delta t$  influences all the  $U_i$  at the next time step, through the solution of the implicit (tridiagonal) system, if the boundary conditions are treated in an implicit way. This can best be seen on the following example of a Euler backward integration of the Beam and Warming scheme

( $\theta = 1, \xi = 0$ ):

$$(1 + \tau \bar{\delta} A_i^n) \Delta U_i = -\tau \bar{\delta} f_i^n \quad (19.1.2)$$

Explicitly the system to solve at each time step is

$$\tau A_{i+1}^n \Delta U_{i+1} + 2\Delta U_i - \tau A_{i-1}^n \Delta U_{i-1} = -\tau (f_{i+1}^n - f_{i-1}^n) \quad (19.1.3)$$

At point  $i = M - 1$ , the equation becomes

$$\tau A_M^n \Delta U_M + 2\Delta U_{M-1} - \tau A_{M-2}^n \Delta U_{M-2} = -\tau (f_M^n - f_{M-2}^n) \quad (19.1.4)$$

and the way the information on  $\Delta U_M$  is introduced will influence the solution algorithm and all the  $\Delta U_i$ . Therefore, the influence of the implementation of the boundary conditions on the behaviour of the scheme may be considered as stronger with implicit methods as compared to explicit schemes.

If all the variables were known at a boundary from the knowledge of the physical input, there would be no difficulty in solving equation (19.1.1). However, this is generally not the case with hyperbolic equations.

The number of physical variables that can be imposed freely at a boundary is dependent on the propagation properties of the system and in particular on the information propagated from the boundary *towards the inside* of the flow region. See Section 16.4.4 for a discussion of these properties.

Since each characteristic direction can be considered as transporting a given information, expressed as a combination of conservative or primitive flow variables, the quantities transported from the inside of the domain towards the boundary will influence and modify the situation along this boundary.

Hence, only variables transported from the boundaries towards the interior can be freely imposed at the boundaries as *physical boundary conditions*. The remaining variables will depend on the computed flow situations and are therefore part of the solution. However, from a numerical point of view, in order to solve for  $U_2^{n+1}$  in equation (19.1.1), that is to compute the solution at the following time step, information about all the components of  $U_1^n$  is required in addition to the allowed physical conditions. This additional information, called *numerical boundary conditions*, has to be consistent with the physical properties of the flow, as well as compatible with the discretized equations.

The number of physical conditions has been defined in Section 16.4.4 as a function of the flow situation at the boundary (see Table 16.1). Since the total number of dependent variables is three in a one-dimensional flow ( $N$  in general), the number  $N_n$  of numerical boundary conditions to be added to the discretized system of equations is equal to

$$N_n = N - N_p \quad (19.1.5)$$

where  $N_p$  is the number of physical conditions.

### 19.1.1 Characteristic boundary conditions

The propagation properties in a one-dimensional flow are expressed in a straightforward way by the characteristic variables, or equivalently by the

Table 19.1. Physical and numerical boundary conditions for one-dimensional flows

	Subsonic	Supersonic
Inlet	Physical conditions: $w_1, w_2$	Physical conditions: $w_1, w_2, w_3$
	Numerical conditions: $w_3$	Numerical conditions: none
Outlet	Physical conditions: $w_3$	Physical conditions: none
	Numerical conditions: $w_1, w_2$	Numerical conditions: $w_1, w_2, w_3$

Riemann invariants. The form of the missing information is therefore defined by the variables associated with the outgoing characteristics (Figures 16.4.7 and 19.1.1).

Table 16.1 can now be completed with the requirements on the numerical boundary conditions, and this is presented in Table 19.1, referring to the notations of Section 16.4 for the characteristic variables  $W$  with components  $w_1, w_2, w_3$ .

Hence, the number as well as the form of the missing information is theoretically known. For instance, at a subsonic outlet, one should impose the characteristic variable  $w_3$  as the physical boundary condition and add, as numerical conditions, the characteristic equations for  $w_1$  and  $w_2$  discretized in a suitable way.

This forms the basis of the *characteristic boundary method*, which adds the Riemann invariants or the compatibility equations for the outgoing characteristics to the imposed physical boundary conditions, in order to obtain the missing equations for points  $i = 1$  and  $i = M$ ; see also Moretti (1981) for a general discussion and earlier references.

For instance, using the Riemann invariants one can apply the following relations at point  $P_1$  of Figure 19.1.1, referring to equations (16.4.33):

$$\left(\frac{p}{\rho^\gamma}\right)_{P_1} = \left(\frac{p}{\rho^\gamma}\right)_{Q_0} \equiv w_1 \quad (19.1.6)$$

$$\left(u + \frac{2c}{\gamma - 1}\right)_{P_1} = \left(u + \frac{2c}{\gamma - 1}\right)_{Q_+} \equiv w_2 \quad (19.1.7)$$

$$\left(u - \frac{2c}{\gamma - 1}\right)_{P_1} \equiv w_3^{(P)} \quad (19.1.8)$$

where the variables at points  $Q_+$  and  $Q_0$  are known, as can be seen from Figure 19.1.1. The quantity  $w_3^{(P)}$  is the imposed physical boundary condition. The system of these three equations determines all the quantities in point  $P_1$  and define the vector  $U_i^{n+1}$  at  $i = M$ .

### 19.1.2 Compatibility relations

An alternative to the characteristic method is to apply the compatibility relations in differential form, discretizing them in an appropriate manner.

For a quasi-one-dimensional nozzle flow of area  $S$ , this would lead to the following equations (see equations (16.4.17)) at the subsonic outlet point  $P_1$  of Figure 19.1.1, assuming  $u > 0$ :

$$\left(\frac{\partial \rho}{\partial t} - \frac{1}{c^2} \frac{\partial p}{\partial t}\right) + u \left(\frac{\partial \rho}{\partial x} - \frac{1}{c^2} \frac{\partial p}{\partial x}\right) = 0 \quad (19.1.9)$$

$$\left(\frac{\partial u}{\partial t} + \frac{1}{\rho c} \frac{\partial p}{\partial t}\right) + (u + c) \left(\frac{\partial u}{\partial x} + \frac{1}{\rho c} \frac{\partial p}{\partial x}\right) = -\frac{uc}{S} \frac{dS}{dx} \quad (19.1.10)$$

$$B(u, \rho, p) = 0 \quad (19.1.11)$$

where  $B(u, \rho, p) = 0$  is the imposed physical boundary condition.

These equations have to be discretized at point  $P_1$ ,  $i = M$ , by using only interior information, that is one has to apply one-sided differencing only. An example of this approach can be found in Steger *et al.* (1980).

This is fully compatible with the mathematical analysis of boundary conditions and of the well-posedness of an initial boundary value problem, as analysed by Kreiss (1968, 1970). Indeed, the scalar hyperbolic equation  $u_t + au_x = 0$  is well posed in the sense of Kreiss, that is the boundary conditions are not over- or underspecified and the solution depends continuously on the initial and boundary data if a boundary condition is imposed at  $x = 0$  when  $a > 0$  and at  $x = L$  when  $a < 0$ .

In addition, the same condition corresponds also to the stability requirements of the upwind differencing. Indeed, as seen in Chapter 10 in Volume 1, the upwind scheme applied at  $i = M$ :

$$u_M^{n+1} = u_M^n - \sigma(u_M^n - u_{M-1}^n) \quad (19.1.12)$$

is stable for  $a > 0$  and  $\sigma < 1$  but unstable for  $a < 0$ , as is easily seen from the Von Neumann amplification factor  $G = 1 - \sigma + \sigma e^{-I\phi}$ .

Since the numerical conditions (19.1.9) and (19.1.10) correspond precisely to the characteristics with positive speeds of propagation, they will be stable under an upwind differencing. On the other hand, the physical boundary condition replaces the negative characteristic which would have been unstable under a backward discretization.

This consistency and harmony between the physical, mathematical and numerical properties is, of course, to be expected but is nevertheless worth mentioning.

The above considerations do not resolve, by far, all the problems connected with the implementation of the boundary conditions. If the characteristic boundary method is the most rigorous one from a physical point of view, various other ways of expressing the information corresponding to the outgoing characteristics can be defined. These are known as *extrapolation* techniques and will be discussed in the following sections. Other forms for the physical boundary conditions can also be defined, such as the *non-reflecting* boundary conditions, which are a particular formulation of the characteristic equations (Engquist and Majda, 1977, 1979; Hedstrom, 1979).

In addition, the Euler equations are generally solved in conservative form, and the physical boundary conditions on the characteristics have to be expressed as a function of the conservative variables. On the other hand, the physical boundary conditions are derived in many cases from experimental set-ups and are given in terms of measurable quantities such as the primitive variables  $\rho$ ,  $u$ ,  $p$ . For instance, the flow conditions in a nozzle are dominated for fixed inlet conditions by the downstream value of the pressure.

Various combinations of primitive or conservative variables have therefore to be selected as physical boundary conditions, raising several questions:

- (1) Which combinations of primitive (or conservative) variables may be applied as physical boundary conditions, in order to reconstruct the information contained in the incoming and outgoing characteristics? If this is not possible, the selected combination leads to an ill-posed problem. This will be investigated in Section 19.1.3.
- (2) What is the interrelation between physical boundary conditions at inlet and at outlet? Is any combination of non-characteristic variables equally valid in defining a well-posed problem with a unique solution? Wornom and Hafez (1984) have pointed out that certain combinations are to be excluded and this will also be discussed in Section 19.1.3.
- (3) What is the influence of the boundary treatment on the stability and accuracy of the basic scheme, also called the *interior scheme*? This is a crucial topic, since stable interior schemes can be strongly affected by unadapted boundary treatments, leading to possible instability of the complete scheme or to the reduction of unconditional to conditional stability. The theoretical analysis of the influence of boundary schemes on stability and accuracy is a difficult task and some results are available for simple problems which will be mentioned in Section 19.1.4.

Most of the research work in the field of the analysis of boundary schemes for initial boundary value problems is of a mathematical and theoretical nature. We refer the interested reader to the important contributions of Kreiss (1968, 1970, 1974); Osher (1969a, 1969b); Gustafsson *et al.* (1972); Gustafsson and Kreiss (1979); Trefethen (1983, 1984, 1985); and to the more complete references listed in these publications and in the review of Higdon (1986).

The non-mathematical-oriented reader will find much benefit in consulting the publications by Yee (1981), Yee *et al.* (1982), Beam *et al.* (1981) and Warming *et al.* (1983), which summarize the state of the art oriented towards the applied numerical scientists and focusing on the applications to the system of Euler equations.

### 19.1.3 Characteristic boundary conditions as a function of conservative and primitive variables

The problem will be well posed if the full information on the ingoing and outgoing characteristics can be recovered from the imposed combinations of

conservative or primitive variables. Since the transformation matrices between the characteristic  $W$ , primitive  $V$  and conservative variables  $U$  are known, it is not difficult to investigate the conditions under which an imposed combination of variables leads to a well-posed problem.

The following transformation matrices between the variables  $W, V$  and  $U$  have been defined in Section 16.4, for arbitrary variations  $\Delta$ :

$$\Delta W = L^{-1} \Delta V \tag{19.1.13}$$

$$\Delta W = L^{-1} M^{-1} \Delta U \equiv P^{-1} \cdot \Delta U \tag{19.1.14}$$

The matrices  $L^{-1}$  and  $P^{-1}$  are given in their one-dimensional form by equations (16.4.9) and (16.4.11). The three set of variables are

$$\Delta W = \begin{pmatrix} \Delta \rho - \frac{1}{c^2} \Delta p \\ \Delta u + \frac{1}{\rho c} \Delta p \\ \Delta u - \frac{1}{\rho c} \Delta p \end{pmatrix} \equiv \begin{pmatrix} \Delta w_1 \\ \Delta w_2 \\ \Delta w_3 \end{pmatrix} \quad U = \begin{pmatrix} \rho \\ \rho u \\ \rho E \end{pmatrix} \quad V = \begin{pmatrix} \rho \\ u \\ p \end{pmatrix} \tag{19.1.15}$$

The well-posedness analysis has to be performed on the linearized equations whereby the coefficients of the matrices  $L^{-1}$  and  $P^{-1}$  are considered as constants, equal to their value on the boundaries. Consequently, the variations  $\Delta$  are small perturbations around the local boundary values, which will be indicated by a subscript 0.

The analysis procedure can be systematized as follows (Yee, 1981). If the transformation matrix, say between  $W$  and  $V$ , is reordered such that the imposed set of physical boundary conditions is separated from the remaining variables, the information along the characteristics corresponding to the numerical boundary condition must allow these remaining variables to be defined. Referring to Figure 19.1.1 and the subsonic outlet point  $P_1$ , one physical boundary condition is allowed, say pressure  $p$ . The transformation relation (19.1.13) is written with the 'physical' characteristic  $w_3$  on top (see Table 19.1):

$$\Delta W \equiv \begin{pmatrix} \Delta w_3 \\ \Delta w_1 \\ \Delta w_2 \end{pmatrix} = \begin{pmatrix} \frac{-1}{\rho c} & 0 & 1 \\ \frac{-1}{c^2} & 1 & 0 \\ \frac{1}{\rho c} & 0 & 1 \end{pmatrix}_0 \cdot \begin{pmatrix} \Delta p \\ \Delta \rho \\ \Delta u \end{pmatrix} \tag{19.1.16}$$

The numerical conditions, obtained from (19.1.16),

$$\Delta w_1 = \frac{-\Delta p}{c_0^2} + \Delta \rho \tag{19.1.17}$$

$$\Delta w_2 = \frac{\Delta p}{\rho_0 c_0} + \Delta u \quad (19.1.18)$$

can clearly be solved for the remaining variables  $\rho$  and  $u$  at the boundary, since  $p$  is known.

Formally writing  $\Delta W^P$  for the characteristics corresponding to the physical boundary conditions and  $\Delta W^N$  for the remaining characteristics defining the numerical information from the interior towards the boundaries, equation (19.1.16) is formalized as follows:

$$\Delta W = \begin{vmatrix} \Delta W^P \\ \Delta W^N \end{vmatrix} = \begin{vmatrix} (L^{-1})_I^P & (L^{-1})_{II}^P \\ (L^{-1})_I^N & (L^{-1})_{II}^N \end{vmatrix} \begin{vmatrix} \Delta V^I \\ \Delta V^{II} \end{vmatrix} \quad (19.1.19)$$

The group of variables  $V^I$  represents the *imposed* physical conditions while the group  $V^{II}$  represents the *free* variables to be defined by the numerical or internal information. The transformation matrix  $L^{-1}$  is subdivided into the appropriate submatrices. In the case of equation (19.1.16) one has  $W^P = w_3$ :

$$W^N = \begin{vmatrix} w_1 \\ w_2 \end{vmatrix} \quad V^I = p \quad V^{II} = \begin{vmatrix} \rho \\ u \end{vmatrix} \quad (19.1.20)$$

and

$$(L^{-1})_I^P = \frac{-1}{\rho c} \quad (L^{-1})_{II}^P = (0, 1) \quad (19.1.21)$$

$$(L^{-1})_I^N = \begin{vmatrix} -1 \\ c^2 \\ 1 \\ \rho c \end{vmatrix} \quad (L^{-1})_{II}^N = \begin{vmatrix} 1 & 0 \\ 0 & 1 \end{vmatrix} \quad (19.1.22)$$

The condition for well-posedness is that  $V^{II}$  can be recovered from the information carried by the characteristics  $W^N$  which intersect the boundary from the interior of the flow domain. Writing

$$\Delta W^N = (L^{-1})_I^N \Delta V^I + (L^{-1})_{II}^N \Delta V^{II} \quad (19.1.23)$$

the free variables  $V^{II}$  are defined by

$$\Delta V^{II} = \frac{1}{(L^{-1})_{II}^N} [\Delta W^N - (L^{-1})_I^N \Delta V^I] \quad (19.1.24)$$

Hence, the condition for well-posedness is that the matrix  $(L^{-1})_{II}^N$  is non-singular, that is the condition of non-zero determinant

$$\det |(L^{-1})_{II}^N| \neq 0 \quad (19.1.25)$$

has to be satisfied. This can be applied for the various combinations of primitive variables at inlet and at outlet.

At a subsonic outlet, equation (19.1.16) shows that any of three variables  $\rho$ ,  $u$ ,  $p$  can be chosen as a physical boundary condition, since none of the submatrices defining  $W^N$  is zero.

*Subsonic inlet*

At a subsonic inlet,  $W^P$  is formed by  $w_1$  and  $w_2$ , while  $W^N = w_3$  and one has

$$\Delta \begin{vmatrix} W^P \\ W^N \end{vmatrix} = \begin{vmatrix} 1 & 0 & \frac{-1}{c^2} \\ 0 & 1 & \frac{1}{\rho c} \\ 0 & 1 & \frac{-1}{\rho c} \end{vmatrix} \cdot \Delta \begin{vmatrix} \rho \\ u \\ p \end{vmatrix} \quad (19.1.26)$$

Since one of the elements of the submatrix defining  $W^N$  (0 1  $-1/\rho c$ ) is zero, namely the element corresponding to the density  $\rho$ , the choice  $(u, p)$  as a physical boundary condition is not well posed. Indeed, since

$$\Delta W^N = \Delta u - \frac{1}{(\rho c)_0} \Delta p \quad (19.1.27)$$

one cannot define  $\Delta \rho$  at the boundary from the information on  $\Delta W^N$ . For any other combination involving  $\rho$  as a physical condition, equation (19.1.27) will allow the determination of the remaining free variable.

The same considerations can be applied to the conservative variables  $U$  and the matrix  $P^{-1}$  instead of  $L^{-1}$ . Examining matrix  $P^{-1}$  (equation (16.4.11)), it is seen that there are no zero elements and hence any possible combination of variables as physical boundary conditions will be well-posed.

This analysis can also be extended to other combination of variables, say  $X$ , by setting up the transformation matrix  $\Delta W = K \cdot \Delta X$  and investigating the submatrices of  $K$  (see Problems 19.1 and 19.2).

At supersonic boundaries, either all or none of the variables have to be imposed and the problem is always well posed.

The above-described procedure defines the allowable combinations of variables at a given boundary without relation to the selection of variables at the other boundary. This question applies only to flow situations that are subsonic at both boundaries and is actually not a trivial question, since it has been observed (Wornom and Hafez, 1984) that certain combinations can give rise to non-unique steady-state solutions.

Wornom and Hafez show that the steady-state subsonic nozzle flow with equal inlet and outlet areas leads to non-unique solutions if the same variable is specified at outlet and at inlet.

This is easily shown from the stationary conservation laws, the subscripts 0 and 1 referring to the two end-points  $x = 0$  and  $x = L$ :

$$(\rho u S)_0 = (\rho u S)_1 \quad (19.1.28)$$

$$H = \left( \frac{\gamma}{\gamma-1} \frac{p}{\rho} + \frac{u^2}{2} \right)_0 = \left( \frac{\gamma}{\gamma-1} \frac{p}{\rho} + \frac{u^2}{2} \right)_1 \quad (19.1.29)$$

$$\left(\frac{p}{\rho^\gamma}\right)_0 = \left(\frac{p}{\rho^\gamma}\right)_1 \quad (19.1.30)$$

If  $\rho$  and  $p$  are imposed at inlet and  $p$  at outlet, that is  $\rho_0$ ,  $p_0$  and  $p_1$  are fixed, the other variables have to be defined from

$$\rho_1^\gamma = \rho_0^\gamma \frac{p_1}{p_0} \quad (19.1.31)$$

$$u_1^2 \left( \frac{\rho_1 S_1}{\rho_0 S_0} - 1 \right) = \frac{2\gamma}{\gamma - 1} \left( \frac{p_1}{\rho_1} - \frac{p_0}{\rho_0} \right) \quad (19.1.32)$$

If the imposed boundary conditions are such that  $p_1 = p_0$ , corresponding to a subsonic inviscid flow without shocks, then  $\rho_1 = \rho_0$  and the right-hand side of equation (19.1.32) vanishes. Hence, the coefficient of  $u_1^2$  has also to be zero in order for a flow to exist. This leaves  $u_1$  undetermined and so the problem is not well posed. Hence, the computed distribution of flow variables will depend on the initial conditions. Therefore, when the flow conditions are identical at the two boundaries, one should not apply the same variable twice as the boundary condition.

*Summarizing*, all combinations of conservative and primitive variables can be selected as physical boundary conditions, with the exception of the pair  $(u, p)$  at a subsonic inlet, if one has to determine the missing information from the characteristic variables. In this case, the imposed conditions should contain the density; for instance,  $(\rho, p)$  or  $(\rho, u)$  are well-posed boundary conditions.

Note, however, that this restriction does not apply with other boundary treatments where the characteristic variables are explicitly determined at the boundaries.

In the particular case of identical subsonic inflow and outflow situations, the outlet boundary condition should contain the third variable, that is  $u_1$  has to be associated with  $(p_0, \rho_0)$  or  $p_1$  has to be coupled to  $(u_0, \rho_0)$ . This restriction is, however, not necessary when the inlet and outlet flow conditions are different.

#### 19.1.4 Extrapolation methods

Next to the direct application of the characteristic and compatibility relations, many other methods can be applied in order to implement numerical boundary conditions.

Various forms are listed below as a sample of the most popular methods, although many other approaches can be defined. They are based on extrapolations of the internal variables towards the boundary.

The listed formulas are at most of first order, which is generally sufficient for second-order schemes, but quadratic extrapolation formulas can be used as well.

The following methods can be applied to any set of variables—conservative, primitive or characteristic—at an inlet or an outlet boundary. In order to stress this fact, we will use the variable  $X$  to represent either  $U, V, W$  or any other

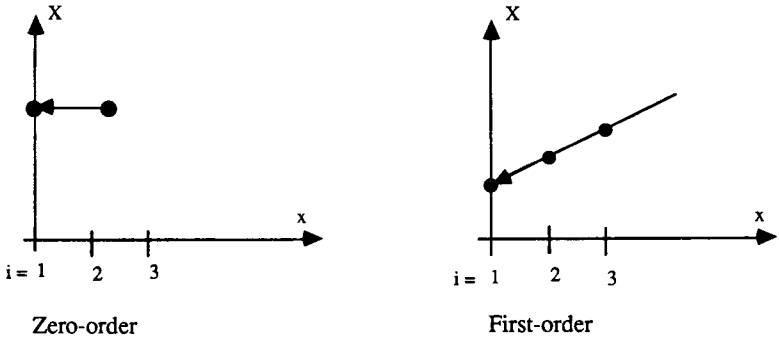


Figure 19.1.2 Illustration of various forms of variable extrapolation. Space extrapolation of variable  $X$  at fixed time

combination, and write the conditions for an outlet boundary  $i = M$ . The transposition to inlet conditions is straightforward, replacing  $i = M$  by  $i = 1$ ,  $i = (M - 1)$  by  $i = 2$  and so on (Figures 19.1.2 to 19.1.4).

### A. Space extrapolation

#### Zero-order extrapolation

$$X_M^{n+1} = X_{M-1}^{n+1} \quad (19.1.33)$$

or

$$\Delta X_M = \Delta X_{M-1} \quad (19.1.34)$$

where

$$\Delta X = X^{n+1} - X^n \equiv \Delta X^n \quad (19.1.35)$$

#### First-order extrapolation

$$X_M^{n+1} = 2X_{M-1}^{n+1} - X_{M-2}^{n+1} \quad (19.1.36)$$

or

$$\Delta X_M^n = 2\Delta X_{M-1}^n - \Delta X_{M-2}^n \quad (19.1.37)$$

### B. Space-time extrapolation

#### Zero order

$$X_M^{n+1} = X_{M-1}^n \quad (19.1.38)$$

or

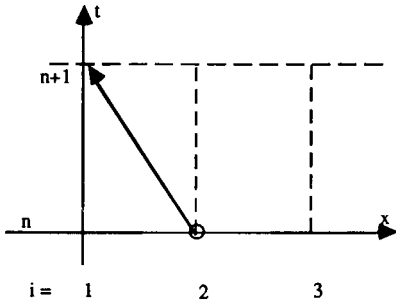
$$\Delta X_M^n = \Delta X_{M-1}^{n-1} \quad (19.1.39)$$

#### First order space/zero order in time

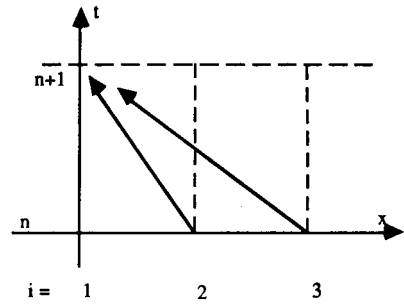
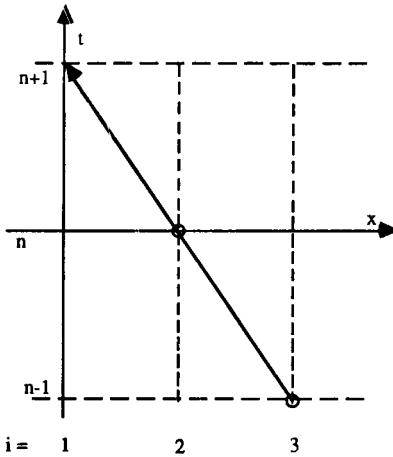
$$X_M^{n+1} = 2X_{M-1}^n - X_{M-2}^n \quad (19.1.40)$$

or

$$\Delta X_M^n = 2\Delta X_{M-1}^{n-1} - \Delta X_{M-2}^{n-1} \quad (19.1.41)$$



Zero order

First order in space / zero  
order in time

First order in space / first order in time

Figure 19.1.3 Illustration of various forms of variable extrapolation. Space-time extrapolation

*First order in space and time*

$$X_M^{n+1} = 2X_{M-1}^n - X_{M-2}^{n-1} \quad (19.1.42)$$

or

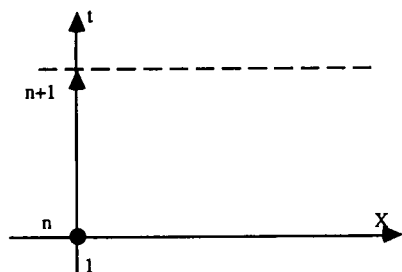
$$\Delta X_M^n = 2\Delta X_{M-1}^{n-1} - \Delta X_{M-2}^{n-2} \quad (19.1.43)$$

*C. Time extrapolation**Zero order*

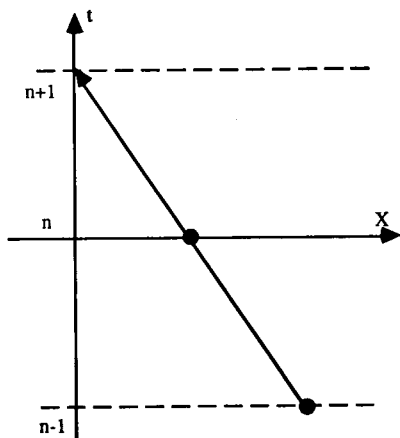
$$X_M^{n+1} = X_M^n \quad (19.1.44)$$

or

$$\Delta X_M^n = 0 \quad (19.1.45)$$



Zero order



First order

Figure 19.1.4 Illustration of various forms of variable extrapolation. Time extrapolation of variable  $X$  at fixed position

### First order

$$X_M^{n+1} = 2X_M^n - X_M^{n-1} \quad (19.1.46)$$

or

$$\Delta X_M^n = \Delta X_M^{n-1} \quad (19.1.47)$$

Note that Figure 19.1.3 is a representation in the space-time plane  $x-t$ , while Figures 19.1.2 and 19.1.4 are representations of the variable  $X$  as a function of space or time.

The space-extrapolation techniques can be considered either as an explicit or as an implicit treatment of the numerical boundary conditions and are adapted to explicit and implicit schemes. On the other hand, the space-time extrapolations are explicit in nature, while the pure time extrapolations are well adapted to implicit (tridiagonal) schemes in  $\Delta$  form.

The extrapolation techniques are discussed in some detail by Griffin and Anderson (1977) and by Gottlieb and Turkel (1978) for applications to the two-step Lax-Wendroff type of schemes, such as the Richtmyer or MacCormack schemes. They show, for instance, that the space-extrapolation methods do not destabilize these schemes nor reduce the stability limits.

With regard to accuracy, an important theorem by Gustafsson (1975) proves that, for linear equations, the boundary scheme can be one order lower than the interior scheme without reducing the global order of accuracy of the complete scheme. Hence, the zero-order space-accurate boundary schemes will reduce the overall accuracy of second-order schemes, while this will not be the case for the first-order boundary scheme.

With regard to implicit methods, the available results can be summarized, following Yee *et al.* (1982), as follows:

- (1) All  $A$ -stable interior schemes remain unconditionally stable with the implicit space extrapolation.
- (2) Coupled to space–time extrapolations, the implicit schemes will tend to lose their unconditional stability. An interesting example is given in the above-mentioned reference of the implicit Euler scheme ( $\theta = 1$ ,  $\xi = 0$ ), which is unconditionally stable for an odd number of mesh points but becomes conditionally stable for an even number of mesh points.
- (3) Generally, when coupled to other implicit boundary schemes, the interior implicit  $A$ -stable schemes remain unconditionally stable, while they reduce to conditional stability when coupled with explicit boundary schemes.

These results are based on linearized theory, but have been generally confirmed by numerical tests on non-linear equations such as Burgers equation and the Euler equations. We note also here that the unconditional stability referred to is to be interpreted as allowing very large CFL values to be applied for steady-state computations. We refer the reader to the cited references for more precise mathematical definitions of the stability criteria.

#### *Another approach*

Another family of numerical boundary conditions consists in discretizing the equations at the boundary points in a one-sided manner and adding this equation to the interior scheme. For instance, considering equation (19.1.1) for the Lax–Wendroff scheme, one could add a first-order appropriate upwind equation for  $U_1$  (see the next chapter for more details on the upwind formulation with mixed sign eigenvalues) and provide in this way the missing information.

### **19.1.5 Practical implementation methods for numerical boundary conditions**

Since the various forms for the numerical boundary conditions can be applied to any of the variables, a large number of non-equivalent formulations can be defined. For instance, a space-extrapolation method can be applied to the conservative variables, as, for instance, Lerat *et al.* (1984), or to the characteristic variables, following Yee *et al.* (1982), or to the primitive variables, or to any other combination of variables. In addition, various forms of extrapolation can be used for any of the above choice of variables. Due to the non-linearity of the flow equations, these choices are not equivalent and lead to different boundary treatments.

As another alternative, one can discretize directly the compatibility equations associated with the outgoing characteristics, or add to the internal scheme a one-sided discretization of the conservation equations or of the non-conservative form of the equations, coupled at the boundary with the physical conditions.

We will describe in this section a few of the methods that can be applied, since it is not possible to cover all the possibilities. We encourage the reader to experiment with as many methods as possible, since the numerical treatment of the boundary conditions is an essential aspect of a numerical simulation.

### *Characteristic extrapolation method*

The transformation between the different set of variables follows the framework described in Section 19.1.2, and we will illustrate it on the example of a space extrapolation on the characteristic variables with a scheme based on the conservative variables and boundary conditions imposed on the primitive variables. This is the method adapted by Yee *et al.* (1982) and is an alternative to the one-sided discretization of the compatibility equations corresponding to the outgoing characteristics.

Referring to equation (19.1.24), the numerical characteristic variables  $\Delta W^N$  are defined by an extrapolation, say equation (19.1.37), where  $\Delta$  represents a time increment:

$$\Delta W^N|_M = 2\Delta W^N|_{M-1} - \Delta W^N|_{M-2} \quad (19.1.48)$$

The values at  $i = (M - 1)$  and  $i = (M - 2)$  are obtained from the primitive variables by an explicit evaluation following equation (19.1.23):

$$\Delta W_i^N = (L_i^{-1})_I^N \cdot \Delta V_i^I + (L_i^{-1})_{II}^N \cdot \Delta V_i^{II} \quad \text{for } i = M - 1, M - 2 \quad (19.1.49)$$

where the matrix elements are evaluated at time level  $n$ . Equation (19.1.24) then gives

$$\Delta V_M^{II} = \frac{1}{(L_M^{-1})_{II}^N} \Delta W_M^N \quad (19.1.50)$$

where  $\Delta V_M^I = 0$  has been introduced since this indicates that the variables  $V_M^I$  are fixed by the physical boundary conditions. In a time-dependent problem  $\Delta V_M^I$  will not be zero and determined by the imposed time variation.

Finally, the free variables  $V_M^{II}$  are transformed to the conservative variables by application of the matrix  $M$ , evaluated at time level  $n$ :

$$\Delta U_M = M_M \begin{vmatrix} \Delta V^I \\ \Delta V_M^{II} \end{vmatrix} = M_M \begin{vmatrix} 0 \\ \Delta V_M^{II} \end{vmatrix} \quad (19.1.51)$$

### *Subsonic outflow boundary, outflow pressure imposed*

Referring to Figure 19.1.1 and equations (19.1.16) to (19.1.22), which define the different submatrices, we have for  $\Delta W^N$  at points  $i = M - 1$  and  $M - 2$ , following equation (19.1.49),

$$\Delta W_i^N \equiv \Delta \begin{vmatrix} w_1 \\ w_2 \end{vmatrix}_i = \begin{vmatrix} -1 \\ c^2 \\ 1 \\ \rho c \end{vmatrix}_i \Delta p_i + \begin{vmatrix} 1 & 0 \\ 0 & 1 \end{vmatrix}_i \Delta \begin{vmatrix} \rho \\ u \end{vmatrix}_i \quad (19.1.52)$$

and

$$\Delta W_M^N = 2 \begin{vmatrix} \frac{-\Delta p}{c^2} + \Delta \rho \\ \frac{\Delta p}{\rho c} + \Delta u \end{vmatrix}_{M-1} - \begin{vmatrix} \frac{-\Delta p}{c^2} + \Delta \rho \\ \frac{\Delta p}{\rho c} + \Delta u \end{vmatrix}_{M-2} = \begin{vmatrix} \Delta w_1 \\ \Delta w_2 \end{vmatrix}_M \quad (19.1.53)$$

The primitive free variables  $\Delta V_M^{\text{II}}$  are obtained from equation (19.1.50) with

$$\frac{1}{(L_M^{-1})_{\text{II}}^M} = \begin{vmatrix} 1 & 0 \\ 0 & 1 \end{vmatrix} \quad (19.1.54)$$

$$\Delta V_M^{\text{II}} = \begin{vmatrix} \Delta \rho \\ \Delta u \end{vmatrix}_M = \begin{vmatrix} 1 & 0 \\ 0 & 1 \end{vmatrix} \begin{vmatrix} \Delta w_1 \\ \Delta w_2 \end{vmatrix}_M \quad (19.1.55)$$

and the corresponding conservative variables are obtained from equation (19.1.51):

$$\Delta U_M = M \begin{vmatrix} \Delta \rho \\ \Delta u \\ 0 \end{vmatrix}_M = \begin{vmatrix} 1 & 0 & 0 \\ u & \rho & 0 \\ \frac{u^2}{2} & \rho u & \frac{1}{\gamma-1} \end{vmatrix}_M \begin{vmatrix} \Delta w_1 \\ \Delta w_2 \\ 0 \end{vmatrix}_M = \begin{vmatrix} \Delta \rho \\ \Delta(\rho u) \\ \Delta(\rho E) \end{vmatrix}_M \quad (19.1.56)$$

where the coefficients of the matrix  $M$  are evaluated at time level  $n$ . One finally obtains the equation, for instance for  $\Delta \rho$ ,

$$\Delta \rho_M + \left( \frac{2\Delta p}{c^2} \right)_{M-1} - 2 \cdot \Delta \rho_{M-1} - \left( \frac{\Delta p}{c^2} \right)_{M-2} + \Delta \rho_{M-2} = 0 \quad (19.1.57)$$

which has to be added to the interior scheme equations written up to the point  $M-1$ .

Equation (19.1.56) can be considered as an explicit or an implicit boundary scheme. For an implicit interior scheme with a tridiagonal matrix structure such as equations (19.1.3) and (19.1.4), the above equation (19.1.57) and the two others for  $\Delta(\rho u)_M$  and  $\Delta(\rho E)_M$  provide the additional equations needed for  $\Delta U_M$ .

An alternative consists in the elimination of  $\Delta U_M$  in equation (19.1.4) by introducing equation (19.1.56) without adding additional equations. One should take care to maintain the block tridiagonal structure of the systems. Indeed, this structure might be lost for some combinations when equations of the form (19.1.57) are added as additional equations.

### Example 19.1.1 MacCormack scheme with time extrapolation of characteristic variables

Consider the original explicit MacCormack scheme under the form (17.2.31)

with the source term  $Q$ :

$$\begin{aligned}\overline{\Delta U}_i &= -\tau(f_{i+1}^n - f_i^n) + \Delta t Q_i^n \\ \overline{\Delta U}_i &= \tau(\bar{f}_i - \bar{f}_{i-1}) + \Delta t \bar{Q}_i \\ \Delta U_i^n &= \frac{1}{2}(\overline{\Delta U}_i + \overline{\Delta U}_i)\end{aligned}\quad (\text{E19.1.1})$$

Boundary conditions are required for each step separately which have to be compatible with the conditions on the global scheme.

The first equation of (E19.1.1) defines the predictor boundary values at the inlet  $\overline{\Delta U}_1$  and the second equation can be used to obtain a corrector boundary value at the outlet  $\overline{\Delta U}_M$ , since the forward predictor step defines  $\Delta U_1$  from the variables in point  $i = 2$  and similarly for the backward corrector at outlet.

In order to obtain global boundary values a predictor boundary correction at the outlet  $\overline{\Delta U}_M$  and a corrector boundary correction at the inlet  $\overline{\Delta U}_1$  are required. Characteristic information at the boundaries together with the physically imposed boundary conditions are applied to calculate  $\overline{\Delta U}_1$  and  $\overline{\Delta U}_M$ .

(a) *Inlet boundary correction  $\overline{\Delta U}_1$*

(i) *Subsonic inlet*

At a subsonic inlet, we select density and pressure as the physical boundary conditions and the velocity  $u$  is to be defined numerically. With

$$\begin{aligned}\rho &= \rho^* && \text{physical boundary condition} \\ p &= p^* && \text{physical boundary condition} \\ u &= u^{\text{num}} && \text{numerical boundary condition}\end{aligned}$$

the characteristic variables at the inlet at the corrector step are defined as follows:

$$\overline{\Delta w}_1 = \overline{\Delta \rho} - \frac{1}{c^2} \overline{\Delta p} \quad (\text{E19.1.2a})$$

$$\overline{\Delta w}_2 = \Delta u^{\text{num}} + \frac{1}{\rho c} \overline{\Delta p} \quad (\text{E19.1.2b})$$

$$\overline{\Delta w}_3 = \Delta w_3^{\text{num}} = \Delta u^{\text{num}} - \frac{1}{\rho c} \overline{\Delta p} \quad (\text{E19.1.2c})$$

The boundary corrections  $\overline{\Delta V}$  for the corresponding primitive variables  $V$  will be consistent if the updating step

$$V^{n+1} = V^n + \frac{1}{2}(\overline{\Delta V} + \overline{\Delta V}) \quad (\text{E19.1.3})$$

maintains the constancy of the imposed variables  $\rho^*$  and  $p^*$ ; that is at a subsonic inlet, the corrector boundary values are related to the imposed variables and

to the calculated predictors at inlet by

$$\overline{\overline{\Delta\rho}} = 2(\rho^* - \rho^n) - \overline{\Delta\rho} \quad (\text{E19.1.4a})$$

$$\overline{\overline{\Delta p}} = 2(p^* - p^n) - \overline{\Delta p} \quad (\text{E19.1.4b})$$

The velocity  $\Delta u_1^{\text{num}}$  is calculated from (E19.1.2c) by the time extrapolation

$$\Delta w_3^{\text{num}} = \overline{\Delta w_3} \quad \text{or} \quad \Delta w_3^{\text{num}} = 0 \quad (\text{E19.1.5})$$

leading to

$$\overline{\overline{\Delta u}} = \Delta u^{\text{num}} = \frac{-1}{\rho c} \overline{\overline{\Delta p}} + \Delta w_3^{\text{num}} \quad (\text{E19.1.6})$$

These corrections are easily transformed into conservative corrections  $\overline{\overline{\Delta U_1}}$ .

Note that generally the initial solution will satisfy the physical boundary conditions and in this case the first terms in equations (E19.1.4) will be zero, that is  $\rho^n = \rho^*$  and  $p^n = p^*$  leading to  $\overline{\overline{\Delta\rho}} = -\overline{\Delta\rho}$  and  $\overline{\overline{\Delta p}} = -\overline{\Delta p}$ .

(ii) *Supersonic inlet*

All three variables are imposed and the boundary corrections can be written directly in terms of conservative variables  $U$ :

$$\overline{\overline{\Delta U_1}} = 2(U_1^* - U_1^n) - \overline{\Delta U_1} \quad (\text{E19.1.7})$$

where  $U_1^*$  is obtained by transforming the physical imposed primitive variables to conservative variables.

(b) *Outlet boundary correction  $\overline{\overline{\Delta U_M}}$*

(i) *Subsonic outlet*

At a subsonic exit, where the pressure is imposed the characteristic predictor values are defined by

$$\overline{\Delta w_1} = \Delta \rho^{\text{num}} - \frac{1}{c^2} \overline{\Delta p} \quad (\text{E19.1.8a})$$

$$\overline{\Delta w_2} = \Delta u^{\text{num}} + \frac{1}{\rho c} \overline{\Delta p} \quad (\text{E19.1.8b})$$

$$\overline{\Delta w_3} = \Delta u^{\text{num}} - \frac{1}{\rho c} \overline{\Delta p} \quad (\text{E19.1.8c})$$

with

$$\overline{\Delta p} = p^* - p^n \quad (\text{E19.1.9})$$

The variables  $\Delta \rho^{\text{num}}$  and  $\Delta u^{\text{num}}$  are calculated from (E19.1.8a) and (E19.1.8b) respectively using a zero-order or first-order extrapolation in time for the corrections  $\overline{\Delta w_1}$  and  $\overline{\Delta w_2}$ ; that is

$$\overline{\Delta w_k^n} = 0 \quad k = 1, 2 \quad \text{zero-order extrapolation} \quad (\text{E19.1.10})$$

$$\overline{\Delta w_k^n} = \Delta w_k^{n-1} \quad k = 1, 2 \quad \text{first-order extrapolation} \quad (\text{E19.1.11})$$

The primitive corrections are then finally given by

$$\overline{\Delta \rho} = \Delta \rho^{\text{num}} = \overline{\Delta w_1} + \frac{1}{c^2} \overline{\Delta p} \quad (\text{E19.1.12})$$

$$\overline{\Delta u} = \Delta u^{\text{num}} = \overline{\Delta w_2} - \frac{1}{\rho c} \overline{\Delta p} \quad (\text{E19.1.13})$$

which are easily transformed to conservative corrections  $\overline{\Delta U_M}$ .

(ii) *Supersonic outlet*

Three numerical boundary conditions have to be imposed. One can directly work with conservative corrections using the following possibilities: a first-order extrapolation in time

$$\overline{\Delta U_N^n} = \Delta U_N^{n-1} \quad (\text{E19.1.14})$$

or a zero-order extrapolation, which gives excellent results,

$$\overline{\Delta U_N^n} = 0 \quad (\text{E19.1.15})$$

*Compatibility relations with time-differenced physical boundary conditions*

This approach, introduced by Chakravarthy (1983), is based on a systematization of the characteristic method, as illustrated by equations (19.1.9) to (19.1.11), whereby the physical boundary conditions are discretized in a time differential form.

The idea behind this formulation relies on the fact that the compatibility relations are obtained by multiplying the conservative Euler equations by the left eigenvectors of the Jacobian matrix  $A$ , as seen in Chapter 16.

At a boundary only the characteristics with negative (outgoing) eigenvalues may be considered, since they provide information from inside the domain, while the characteristics with positive eigenvalues have to be replaced by the physical boundary conditions. Hence at a boundary the matrix  $P^{-1}$ , grouping the left eigenvectors as lines, will have the lines associated with the incoming characteristics zeroed out, in order to maintain only valid information. The remaining equations can be derived from the physical boundary conditions by differentiation in order to define a system of three by three equations at a boundary, which is to be added to the system applied at the internal points.

With the notation of equation (19.1.19), the characteristic compatibility equations (16.4.19) can be written as

$$\frac{\partial}{\partial t} \begin{vmatrix} W^P \\ W^N \end{vmatrix} + \Lambda \frac{\partial}{\partial x} \begin{vmatrix} W^P \\ W^N \end{vmatrix} = L^{-1} \tilde{Q} = P^{-1} Q \quad (\text{19.1.58})$$

or with (16.3.39), as a function of the conservative variables, as

$$\frac{\partial}{\partial t} \left| \frac{W^P}{W^N} \right| + \left| \frac{(P^{-1})^P}{(P^{-1})^N} \right| A \frac{\partial}{\partial x} \left| \frac{U^I}{U^II} \right| = P^{-1} Q \quad (19.1.59)$$

where  $A$  is the Jacobian of the conservative variables. Note that the factor  $A \partial U / \partial x$  can be replaced by the conservative flux derivative  $\partial f / \partial x$ .

Following the procedure described by equations (19.1.9) to (19.1.11), the variables  $W^P$ , which correspond to incoming characteristics, have to be replaced by the physical boundary conditions  $B(U) = 0$ , where  $U$  stands for the conservative variables, for instance.

A fully combined treatment is obtained by taking the time derivative of the boundary conditions

$$\frac{\partial B}{\partial t} = 0 = \frac{\partial B}{\partial U} U, \quad (19.1.60)$$

where  $\partial B / \partial U$  is the Jacobian matrix of the  $B$  functions with respect to  $U$ . Introducing this equation for the physical boundary terms, the full system at the boundaries then becomes

$$\frac{\partial}{\partial t} \left| \frac{B}{W^N} \right| + \Lambda \frac{\partial}{\partial x} \left| \frac{0}{W^N} \right| = \left| \frac{0}{(P^{-1})^N} \right| Q \quad (19.1.61)$$

or with  $\Delta W = P^{-1} \Delta U$ ,

$$\left| \frac{\frac{\partial B}{\partial U}}{(P^{-1})^N} \right| \frac{\partial U}{\partial t} + \left| \frac{0}{(P^{-1})^N} \right| A \frac{\partial U}{\partial x} = \left| \frac{0}{(P^{-1})^N} \right| Q \quad (19.1.62)$$

Explicitly, the equations (19.1.62) are discretized after isolating  $\partial U / \partial t$  in the following way. Defining the two matrices  $P_1, P_2$ ,

$$P_1 = \left| \frac{\frac{\partial B}{\partial U}}{(P^{-1})^N} \right| \quad (19.1.63)$$

$$P_2 = \left| \frac{0}{(P^{-1})^N} \right| \quad (19.1.64)$$

the equations (19.1.62) are discretized after multiplication by  $P_1^{-1}$ , which is non-singular by construction as a consequence of the well-posedness of the selected boundary treatment:

$$\frac{\partial U}{\partial t} + (P_1^{-1} P_2 A) \frac{\partial U}{\partial x} = (P_1^{-1} P_2) Q \quad (19.1.65)$$

or

$$\frac{\partial U}{\partial t} + P_1^{-1} P_2 \frac{\partial f}{\partial x} = (P_1^{-1} P_2) Q \quad (19.1.66)$$

The system (19.1.66) can be discretized in relation to the considered scheme, that is explicitly or implicitly. In both cases, the flux term  $\partial f/\partial x$  will have to be differenced in a one-sided way, forward at an inlet boundary and backward at an outlet section.

When an implicit scheme is selected, these equations can be discretized as follows, with  $P^* \equiv P_1^{-1}P_2$ , in the line of the Beam and Warming schemes:

$$(1 + \tau P^* \delta^- A^n)_M \Delta U_M^n = P_1^{-1} (P_2 Q)_M^n - \tau P^* \delta^- f_M^n \quad (19.1.67)$$

for an outflow boundary and a similar equation at the inflow boundary with a forward differencing operator  $\delta^+$  instead of  $\delta^-$ .

The examples shown in Figure 18.1.6 to 18.1.8 have been obtained with this treatment of the boundary conditions and a first-order upwind discretization of (19.1.67). Note that equation (19.1.67) can also be applied with a second-order backward difference, leading to a second-order accurate boundary scheme.

It is to be noted that the boundary equations (19.1.65) and (19.1.66) are not in conservation form and, furthermore, the upwind discretization at the boundaries is not consistent with the interior scheme from the point of view of global conservation. For instance, if the interior scheme is based on a central differencing of the fluxes  $\bar{\delta} f_i$  and if at the boundary one would apply a first-order upwind formula  $\delta^- f_i = f_i - f_{i-1}$ , this would leave a conservation error of  $(f_{M-1} + f_M)/2 + (f_M - f_{M-1}) = (3f_M - f_{M-1})/2$ . For strict conservation the sum  $\sum_{i=1}^{M-1} \bar{\delta} f_i + (\delta^- f_M)$  should depend only on  $f_1$  and  $f_M$  and not on the fluxes at interior points.

For the implicit schemes of Lerat (Section 17.4) with  $\alpha = 0$ , the explicit step is the physical one, and will require a correct boundary treatment of an explicit nature. The implicit step, being of a mathematical nature, can allow a simplified treatment, such as  $\Delta U = 0$  at the boundaries.

*Example 19.1.2 Subsonic outlet boundary, imposed exit pressure*

The method just described is applied to a subsonic exit section, with imposed pressure, directly in the conservative variables. The matrix  $P^{-1}$  (equation (16.4.11)) is split as follows, keeping the usual order of the equations, that is writing first  $(P^{-1})^N$ :

$$P^{-1} = \begin{vmatrix} (P^{-1})^N \\ (P^{-1})^P \end{vmatrix} \equiv \begin{vmatrix} 1 - \frac{\gamma - 1}{2} \frac{u^2}{c^2} & (\gamma - 1) \frac{u}{c^2} & -\frac{\gamma - 1}{c^2} \\ \left( \frac{\gamma - 1}{2} u^2 - uc \right) \frac{1}{\rho c} & [c - (\gamma - 1)u] \frac{1}{\rho c} & \frac{\gamma - 1}{\rho c} \\ \hline -\left( \frac{\gamma - 1}{2} u^2 + uc \right) \frac{1}{\rho c} & (c + (\gamma - 1)u) \frac{1}{\rho c} & -\frac{\gamma - 1}{\rho c} \end{vmatrix} \quad (E19.1.16)$$

The condition  $B(U) = 0$  is given by

$$B(U) = p - p_1 = 0 \quad (\text{E19.1.17})$$

where  $p_1$  is a constant. The Jacobian  $\partial B/\partial U$  is actually formed by the last line of the matrix  $M^{-1}$ :

$$\frac{\partial B}{\partial U} = \left| \begin{array}{ccc} \frac{\gamma-1}{2} u^2 & -(\gamma-1)u & \gamma-1 \end{array} \right| \quad (\text{E19.1.18})$$

The matrices  $P_1$  and  $P_2$  are defined here as

$$P_1 = \left| \begin{array}{c} (P^{-1})^N \\ \frac{\partial B}{\partial U} \end{array} \right| = \left| \begin{array}{ccc} 1 - \frac{\gamma-1}{2} \frac{u^2}{c^2} & (\gamma-1) \frac{u}{c^2} & -\frac{\gamma-1}{c^2} \\ \left( \frac{\gamma-1}{2} u^2 - uc \right) \frac{1}{\rho c} & [c - (\gamma-1)u] \frac{1}{\rho c} & \frac{\gamma-1}{\rho c} \\ \frac{\gamma-1}{2} u^2 & -(\gamma-1)u & \gamma-1 \end{array} \right| \quad (\text{E19.1.19})$$

$$P_2 = \left| \begin{array}{c} (P^{-1})^N \\ 0 \end{array} \right| = \left| \begin{array}{ccc} 1 - \frac{\gamma-1}{2} \frac{u^2}{c^2} & (\gamma-1) \frac{u}{c^2} & -\frac{\gamma-1}{c^2} \\ \left( \frac{\gamma-1}{2} u^2 - uc \right) \frac{1}{\rho c} & [c - (\gamma-1)u] \frac{1}{\rho c} & \frac{\gamma-1}{\rho c} \\ 0 & 0 & 0 \end{array} \right| \quad (\text{E19.1.20})$$

The matrix  $P^* = P_1^{-1} P_2$  is derived by direct algebraic manipulations:

$$P^* = \left| \begin{array}{ccc} 1 - \frac{\gamma-1}{2} \frac{u^2}{c^2} & (\gamma-1) \frac{u}{c^2} & \frac{1-\gamma}{c^2} \\ \frac{\gamma-1}{2c} u^2 \left( 1 - \frac{u}{c} \right) & 1 + \frac{\gamma-1}{c} u \left( \frac{u}{c} - 1 \right) & \frac{\gamma-1}{c} \left( 1 - \frac{u}{c} \right) \\ -\frac{u^2}{2} \left[ 1 + (\gamma-1) \frac{u}{c} \left( \frac{u}{2c} - 1 \right) \right] & u \left[ 1 + (\gamma-1) \frac{u}{c} \left( \frac{u}{2c} - 1 \right) \right] & -(\gamma-1) \frac{u}{c} \left( \frac{u}{2c} - 1 \right) \end{array} \right| \quad (\text{E19.1.21})$$

### Example 19.1.3 Subsonic inlet—pressure and density fixed

There is only one numerical boundary condition corresponding to the third characteristic. In this case,  $(P^{-1})^N$  and  $(P^{-1})^P$  are reversed in comparison to the previous example and we have

$$B(U) = \left| \begin{array}{c} \rho - \rho^* \\ p - p^* \end{array} \right| = 0 \quad (\text{E19.1.22})$$

where  $\rho^*$  and  $p^*$  are the imposed values.

The Jacobian  $\partial B/\partial U$  is formed by the second and last rows of  $M^{-1}$ :

$$\frac{\partial B}{\partial U} = \begin{vmatrix} 1 & 0 & 0 \\ \frac{\gamma-1}{2}u^2 & -(\gamma-1)u & (\gamma-1) \end{vmatrix} \quad (\text{E19.1.23})$$

The matrices  $P_1$  and  $P_2$  become

$$P_1 = \begin{vmatrix} 1 & 0 & 0 \\ \frac{\gamma-1}{2}u^2 & -(\gamma-1)u & \gamma-1 \\ -\left(\frac{\gamma-1}{2}u^2 + uc\right)\frac{1}{\rho c} & [c + (\gamma-1)u]\frac{1}{\rho c} & -\frac{\gamma-1}{\rho c} \end{vmatrix} \quad (\text{E19.1.24})$$

$$P_2 = \begin{vmatrix} 0 & 0 & 0 \\ 0 & 0 & 0 \\ -\left(\frac{\gamma-1}{2}u^2 + uc\right)\frac{1}{\rho c} & [(c + (\gamma-1)u)]\frac{1}{\rho c} & -\frac{\gamma-1}{\rho c} \end{vmatrix} \quad (\text{E19.1.25})$$

The matrix  $P^* = P_1^{-1}P_2$  is derived by direct algebraic manipulations:

$$P^* = \begin{vmatrix} 0 & 0 & 0 \\ -u\left(1 + \frac{\gamma-1}{2c}u\right) & 1 + (\gamma-1)\frac{u}{c} & -\frac{\gamma-1}{c} \\ -u^2\left(1 + \frac{\gamma-1}{2c}u\right) & \left[1 + (\gamma-1)\frac{u}{c}\right] & -\frac{\gamma-1}{c}u \end{vmatrix} \quad (\text{E19.1.26})$$

*Example 19.1.4 Application to MacCormack and Beam and Warming schemes*

Equation (19.1.66) is written with  $P^* = P_1^{-1}P_2$ :

$$\frac{\partial U}{\partial t} + P^* \frac{\partial f}{\partial x} = P^* Q \quad (\text{E19.1.27})$$

This equation, valid at the boundaries, will be discretized in a one-sided way. A first-order explicit scheme seems to be a good choice, since it has to be combined with the explicit MacCormack scheme.

For an inlet boundary  $i = 1$  one would write

$$\Delta U_1^n = -\tau P_1^* \delta^+ f_1^n + \Delta t P_1^* Q_1^n \quad (\text{E19.1.28})$$

and for an outlet boundary  $i = M$ ,

$$\Delta U_M^n = -\tau P_M^* \delta^- f_M^n + \Delta t P_M^* Q_M^n \quad (\text{E19.1.29})$$

For the Beam and Warming scheme, equation (E19.1.27) is discretized in an implicit way with one-sided differences.

For an inlet boundary  $i = 1$  we have, with an implicit treatment of the source term where  $C = \partial Q / \partial U$  is here the Jacobian of the source term.

$$(1 + \tau P_1^* \delta^+ A_1^n - \Delta t P_1^* C_1^n) \Delta U_1^n = -\tau P_1^* \delta^+ f_1^n + \Delta t P_1^* Q_1^n \quad (\text{E19.1.30})$$

For an outlet boundary  $i = M$ ,

$$(1 + \tau P_M^* \delta^- A_M^n - \Delta t P_M^* C_M^n) \Delta U_M^n = -\tau P_M^* \delta^- f_M^n + \Delta t P_M^* Q_M^n \quad (\text{E19.1.31})$$

Equations (E19.1.30) and (E19.1.31) represent the extra boundary equations completing the blocktridiagonal system of Beam and Warming. More explicitly they can be written as follows:

$$Y \Delta U_1^n + Z \Delta U_2^n = \text{RHS}_1 \quad \text{inlet boundary} \quad (\text{E19.1.32})$$

with

$$\begin{aligned} Y &= 1 - \tau P_1^* A_1^n - \Delta t P_1^* C_1^n \\ Z &= \tau P_1^* A_2^n \\ \text{RHS}_1 &= -\tau P_1^* (f_2^n - f_1^n) + \Delta t P_1^* Q_1^n \end{aligned} \quad (\text{E19.1.33})$$

At the outlet boundary

$$X \Delta U_{M-1}^n + Y \Delta U_M^n = \text{RHS}_M \quad \text{outlet boundary} \quad (\text{E19.1.34})$$

with

$$\begin{aligned} Y &= 1 + \tau P_M^* A_M^n - \Delta t P_M^* C_M^n \\ X &= -\tau P_M^* A_{M-1}^n \\ \text{RHS}_M &= -\tau P_M^* (f_M^n - f_{M-1}^n) + \Delta t P_M^* Q_M^n \end{aligned} \quad (\text{E19.1.35})$$

In general, since the physical boundary conditions are imposed as time derivatives  $\partial_t B = 0$  and linearized as equation (19.1.60), the non-linearity of the boundary conditions will lead to small errors on the exact condition  $B(U) = 0$ . Hence, it is recommended to update the imposed variables, for instance pressure in Example 19.1.1, after each time step in order to satisfy exactly the imposed values. An alternative to the updating, which is actually more consistent with an implicit approach, is to replace equation (19.1.60) by a Newton iteration

$$B(U^{n+1}) = B(U^n) + \frac{\partial B}{\partial U} (U^{n+1} - U^n) \quad (\text{19.1.68})$$

which is a discretized form of equation (19.1.60). Under the condition that the solution at time step  $n + 1$  satisfies exactly the boundary condition  $B(U^{n+1}) = 0$ , equation (19.1.68) can be written with the boundary residual in the right-hand side as

$$\left( \frac{\partial B}{\partial U} \right)^n \Delta U^n = -B(U^n) \quad (\text{19.1.69})$$

This can easily be introduced in equations (19.1.61) to (19.1.67) by adding to the right-hand side the matrix  $\begin{vmatrix} -B \\ 0 \end{vmatrix}$ , leading to the following equation, instead of (19.1.62):

$$\left| \frac{\partial B}{\partial U} \right|_{(P^{-1})^N} \frac{\partial U}{\partial t} + \left| \begin{matrix} 0 \\ (P^{-1})^N \end{matrix} \right| A \frac{\partial U}{\partial x} = \left| \begin{matrix} -B \\ (P^{-1})^N Q \end{matrix} \right| \quad (19.1.70)$$

and equation (19.1.66) becomes

$$\frac{\partial U}{\partial t} + P_1^{-1} P_2 \frac{\partial f}{\partial x} = P_1^{-1} \left| \begin{matrix} -B \\ (P^{-1})^N Q \end{matrix} \right| \quad (19.1.71)$$

In the discretized form of equation (19.1.67), this modification leads to the boundary scheme

$$(1 + \tau P^* \delta^- A^n)_M \Delta U_M^n = -\tau P^* \delta^- f_M^n + P_1^{-1} \left| \begin{matrix} -B^n \\ (P^{-1})^N Q \end{matrix} \right| \quad (19.1.72)$$

The first group of equations are in fact  $B(U) = 0$  at time level  $n$ .

A comparison between this last method and the implicit characteristic extrapolation method is shown in Figures 19.1.5 and 19.1.6. They correspond to the same case and the same conditions as Figure 18.1.7, in particular the same physical boundary conditions, identical CFL numbers of 40 and the same artificial dissipation coefficients. The convergence rates of the three cases are practically identical, reaching a residual reduction of eight orders of magnitude in 100 time steps.

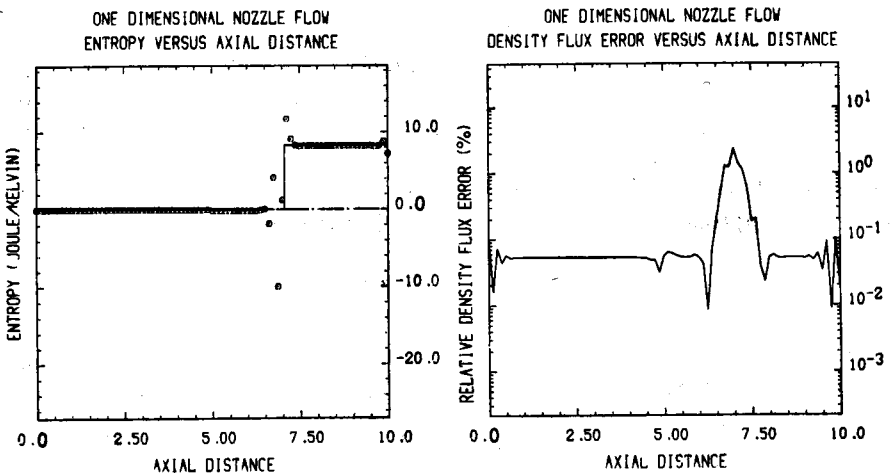


Figure 19.1.5 Mass flux error and entropy distribution obtained with the Beam and Warming scheme and first-order characteristic extrapolation as boundary treatment

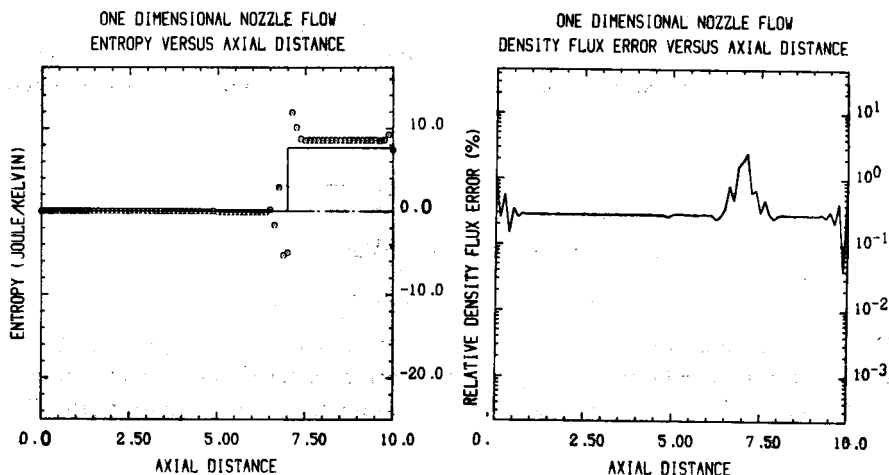


Figure 19.1.6 Mass flux error and entropy distribution obtained with the Beam and Warming scheme and zero-order characteristic extrapolation as boundary treatment

Figure 18.1.7 is obtained with the implicit characteristic treatment, while Figure 19.1.5 and 19.1.6 show the error evolution and entropy plots for the first-order extrapolation on the characteristic variables and the zero-order extrapolation respectively.

The results of Mach and density distributions can not be distinguished from those shown in Figure 18.1.7, but the error curves show an increase in the error level of the density flux which remains limited for the first-order extrapolation but reaches one order of magnitude for the zero-order extrapolation. This is to be expected since Gustafsson's theorem predicts that the coupling of a second-order accurate interior scheme with a zero-order boundary treatment reduces the overall order of accuracy of the complete scheme. This can also be seen on the entropy variation which shows an increased error in the region downstream of the shock.

### 19.1.6 Non-reflecting boundary conditions

This approach is an alternative for the expression of *physical* boundary conditions.

When imposing a constant pressure at a subsonic exit section under the form  $p^{n+1} = p^*$  or  $\Delta p = 0$ , where  $\Delta p = p^{n+1} - p^n = p^* - p^n$  as considered in Examples 19.1.1 and 19.1.2, one actually allows perturbation waves to be reflected at the boundaries. Indeed, since the amplitude of the local perturbation wave carried by the incoming characteristic is  $\Delta w_3 = \Delta u - \Delta p / \rho c$ , imposing  $\Delta p = 0$  amounts to the generation of an incoming wave of intensity  $\Delta w_3 = \Delta u$  reflected from the exit boundary.

The non-reflecting boundary condition (Engquist and Majda, 1977; Hedstrom, 1979) expresses the physical boundary conditions as the requirement that the local perturbations propagated along incoming characteristics be made to vanish: that is

$$\frac{\partial w_k}{\partial t} = 0 \quad \text{for all } k \text{ such that } \lambda_k \text{ enters the domain} \quad (19.1.73)$$

In discretized form this condition is expressed as

$$\Delta w_k = 0 \quad \text{for all } k \text{ such that } \lambda_k \text{ enters the domain} \quad (19.1.74)$$

This condition is automatically satisfied with the characteristic approach (19.1.6) to (19.1.8), but it can be applied with other treatments of the numerical boundary conditions (see Problems 19.6 and 19.7). For a subsonic outlet, equation (19.1.74) becomes

$$\Delta w_3 = \Delta u - \frac{\Delta p}{\rho^n c^n} = 0 \quad (19.1.75)$$

For a subsonic inlet, the non-reflecting boundary conditions would be

see (16.4.18) p. 162

$$\begin{aligned} \Delta w_1 &= \Delta \rho - \frac{\Delta p}{c^{2n}} = 0 \\ \Delta w_2 &= \Delta u + \frac{\Delta p}{\rho^n c^n} = 0 \end{aligned} \quad (19.1.76)$$

It is to be noted that this reasoning remains valid as long as shocks do not cross the boundary, since the characteristic variables are not constant across a shock. Hence the above conditions will generate a reflection when a shock passes through a boundary. However, if the shock is of strength  $\epsilon$ , the Riemann variables change by an amount  $O(\epsilon^2)$  through the shock and produce a reflection of this order of magnitude (Hedstrom, 1979).

In the presence of source terms, the characteristic equations are defined by equation (16.4.19) or

$$\frac{\partial w_k}{\partial t} + \lambda_k \frac{\partial w_k}{\partial x} = l^{(k)} Q \quad (19.1.77)$$

where  $l^{(k)}$  is the left eigenvector of the Jacobian associated with  $\lambda_k$ . At a fixed position of the inlet or outlet boundaries, equation (19.1.73) is generalized as

$$\frac{\partial w_k}{\partial t} = l^{(k)} Q \quad \text{for all } k \text{ such that } \lambda_k \text{ enters the domain} \quad (19.1.78)$$

For a nozzle of cross-section  $S(x)$ , equation (19.1.75) for a subsonic exit becomes

see (16.4.21)

$$\Delta w_3 = \Delta u - \frac{\Delta p}{\rho^n c^n} = \frac{1}{S} \frac{dS}{dx} u^n c^n \quad (19.1.79)$$

Computations show, in particular with unsteady flows but also for stationary conditions, that this procedure provides an improved accuracy at the boundaries and we refer to the listed references for specific examples; see also Thompson (1987) for additional examples.

In steady-state computations and an imposed pressure at a subsonic exit, the non-reflecting condition (19.1.75) does not ensure that  $p = p^*$ , and a strict application of this equation might lead to a steady state depending on the initial data. An *ad hoc* cure to this situation has been proposed by Rudy and Strickwerda (1980). It consists in replacing equation (19.1.73) for the incoming characteristic by the condition  $\alpha > 0$ :

$$\frac{\partial u}{\partial t} - \frac{1}{\rho c} \frac{\partial p}{\partial t} - \frac{\alpha}{\rho c} (p - p^*) = 0 \quad \text{at } i = M \quad (19.1.80)$$

For any finite value of  $\alpha$  the steady-state solution will satisfy the condition  $p = p^*$ .

The parameter  $\alpha$  has to be optimized and some guidelines are provided by Rudy and Strickwerda (1980). For the two-dimensional test cases analysed by these authors with the MacCormack scheme, the convergence rate to steady state was strongly dependent on the parameter  $\alpha$ . The optimum value of  $\alpha$  decreases with increasing Mach number, from roughly 0.1 to 0.2 at Mach number 0.8 to a value close to 1 for Mach numbers of 0.4. However, these values are strongly problem dependent. In any case, the convergence rate was considerably better compared to the case where the condition  $p = p^*$  at exit was used.

Equation (19.1.80) can be discretized in an implicit way, leading to

$$\Delta p_M = (\rho^n c^n \Delta u + \alpha \Delta t \Delta p^*)_M \frac{1}{1 + \alpha \Delta t} \quad (19.1.81)$$

where  $\Delta p = p^{n+1} - p^n$  and  $\Delta p^* = p^* - p^n$ , or in an explicit way

$$\Delta p_M = (\rho^n c^n \Delta u + \alpha \Delta t \Delta p^*)_M \quad (19.1.82)$$

Better results are obtained with the implicit form (19.1.81).

An interesting combination for the expression of boundary conditions, in particular for unsteady problems, is to combine the compatibility equations for the outgoing waves with the non-reflective condition for the incoming characteristics. This corresponds to an application of the procedure developed in Section 19.1.5 with the replacement of the equation  $\partial B / \partial t = 0$  by equation (19.1.78). This replacement maintains equation (19.1.65) with  $P_1 = P^{-1}$ , the complete diagonalization matrix of the Jacobian (E19.1.16). A straightforward interpretation of the equation obtained in this way can be given in terms of flux splitting concepts and will be discussed in Section 20.2.4.

Note that, for stationary problems, equation (19.1.80) might be used in this approach, instead of (19.1.78).

## 19.2 MULTI-DIMENSIONAL BOUNDARY TREATMENT

Multi-dimensional flows contain a variety of boundaries, which can be grouped into:

- (1) Free surfaces, either far-field boundaries in external flows or inlet and outlet sections of internal flow systems (Figures 19.2.1 and 19.2.2).

These are the boundaries through which the flow enters or leaves the computational domain. In external flow problems, free boundaries are generally located far enough from the body such that free-stream conditions can be considered although, as will be seen next, higher accuracy is obtained when some far-field corrections, taking into account the finite distance between the body and the outer boundaries of the computational domain, are introduced.

In internal flow systems, ducts or cascades, these boundaries refer to the inlet and outlet surfaces. For cascades, one has in addition periodic surfaces, resulting from the periodicity of the cascade geometry. These surfaces are not to be considered as external boundaries, since the periodicity condition of equality of all physical flow quantities at corresponding points E, F results in treating these points as internal points, without other boundary treatment.

- (2) Solid body surfaces, either bodies immersed in a flow or bounding walls in ducts and cascades.

### 19.2.1 Physical and numerical boundary conditions

In all cases, the number of physical boundary conditions to be imposed at the boundary surfaces is determined by the characteristic properties.

Referring to the presentation in Section 16.5, the number of physical conditions to be imposed at a boundary with the normal vector  $\vec{n}$  pointing towards the flow domain is defined by the signs of the eigenvalues of the matrix

$$K = \vec{A} \cdot \vec{I}_n = A\hat{n}_x + B\hat{n}_y \quad (19.2.1)$$

where  $\vec{I}_n$  is the unit vector normal to the surface, with components  $(\hat{n}_x, \hat{n}_y)$  in a two-dimensional Cartesian coordinate system.

Remember that  $A$  and  $B$  are the Jacobians of the conservative  $x$  and  $y$  components of the flux vector, with respect to the conservative variables. The matrix

$$\tilde{K} = \vec{A} \cdot \vec{I}_n = \tilde{A}\hat{n}_x + \tilde{B}\hat{n}_y \quad (19.2.2)$$

formed by the Jacobians of the flux components with respect to the primitive variables has the same eigenvalues.

The eigenvalues of the matrix  $K$  are  $\vec{v} \cdot \vec{I}_n$ ,  $\vec{v} \cdot \vec{I}_n$ ,  $\vec{v} \cdot \vec{I}_n + c$ ,  $\vec{v} \cdot \vec{I}_n - c$  in a two-dimensional flow.

The first two eigenvalues are equal to the normal component of the velocity vector,  $v_n$ . The two remaining eigenvalues are associated with the acoustic waves

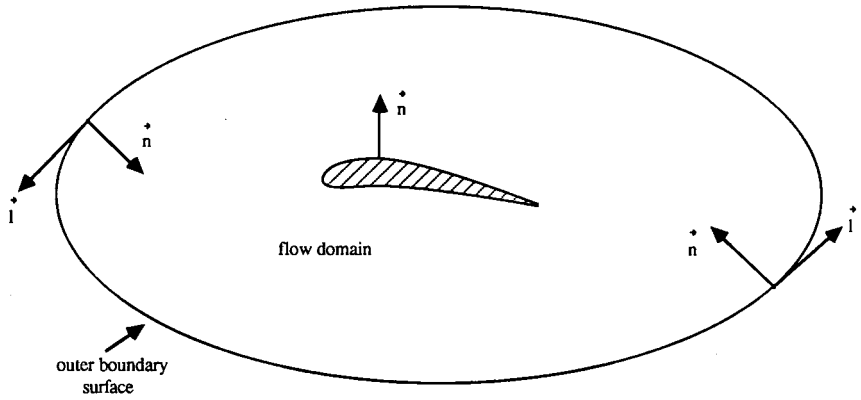
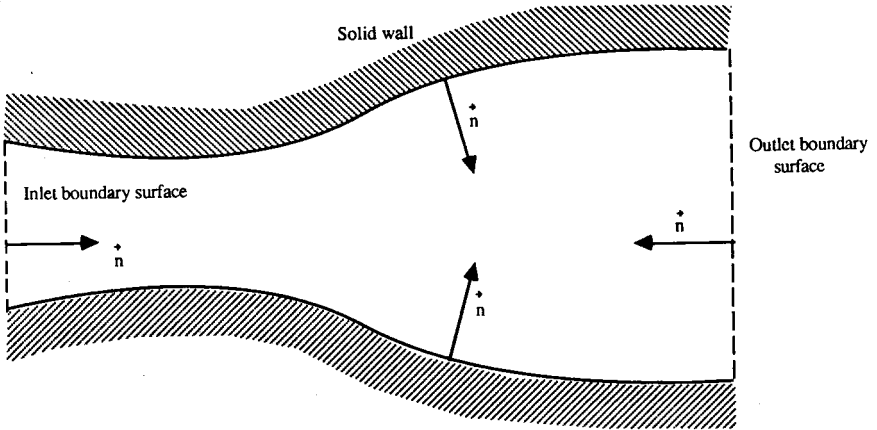
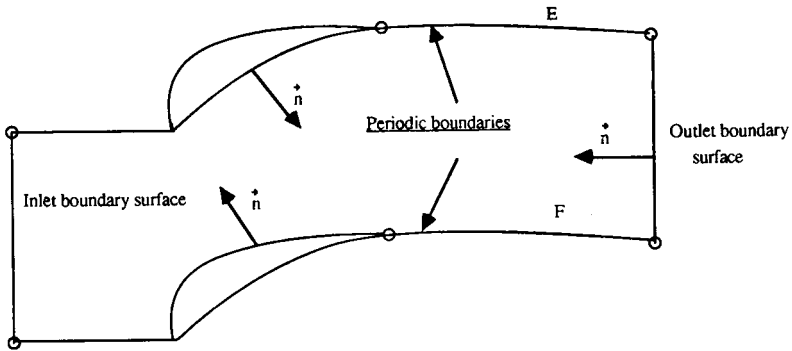


Figure 19.2.1 External flow boundary configuration



(a) Duct flow



(b) Cascade flow

Figure 19.2.2 Internal flow boundary configuration

and are equal to  $v_n \pm c$ . Hence the sign of these eigenvalues will be determined by the velocity components normal to the boundary surfaces.

Note that in a three-dimensional flow, the eigenvalue  $v_n$  appears three times.

The associated wave propagation speeds in the direction  $\bar{l}_n$  are  $\lambda \cdot \bar{l}_n$  where  $\lambda$  represents any of the above eigenvalues, according to equation (16.3.11). Hence, when  $\lambda$  is positive, the information carried by the associated characteristics propagates *from the boundary towards* the interior of the flow domain and a physical boundary condition has to be imposed.

On the other hand, when the eigenvalue  $\lambda$  is negative, information is propagated from the flow domain towards the boundary, influencing thereby the boundary surface conditions. These effects have therefore to be expressed numerically, through numerical boundary conditions.

If the *inlet flow* is subsonic in the direction *normal* to the entry surface, three eigenvalues are positive (four in a three-dimensional situation) and one is negative. Therefore, three (or four) quantities will have to be fixed by the physical flow conditions at the inlet of the flow domain, while the remaining one will be determined by the interior conditions, through a numerical boundary condition (Figure 19.2.3).

Two thermodynamic variables will generally be determined by the upstream stagnation conditions. Most currently, stagnation pressure and temperature can be imposed, or, equivalently, entropy and stagnation enthalpy. The third (and fourth) physical variable(s) will be defined by one (or two) velocity component(s). The remaining velocity component will result from the numerical boundary treatment.

An equivalent option often applied in internal flows, such as channels or cascade computations, is to specify inlet Mach number or velocity magnitude, and have the inlet flow angle defined by the computed flow, or, inversely, fix the incident flow angle, determining inlet Mach number from the computed flow.

In addition, when the flow is choked, that is when the sonic velocity is reached in a minimum area section which is lower than, or equal to, the critical section the mass flow rate cannot be imposed, but has to be calculated from the flow properties through a numerical procedure.

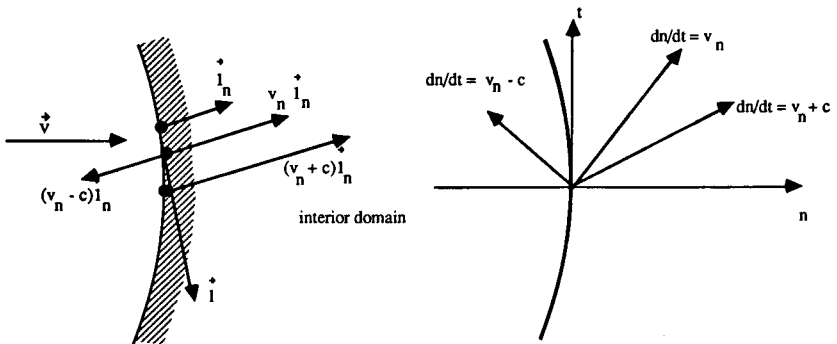


Figure 19.2.3 Subsonic inlet boundary in two-dimensional flows

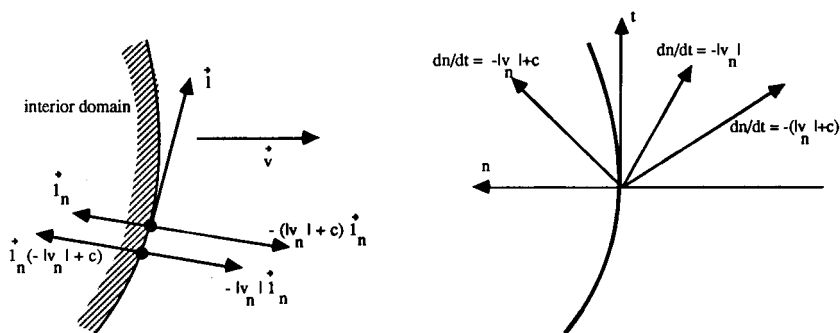


Figure 19.2.4 Subsonic outlet boundary in two-dimensional flows

At an *outlet boundary*, with subsonic normal velocity, three (four) eigenvalues are negative, since the normals are defined as pointing towards the interior flow domain. Three (four) numerical boundary conditions have therefore to be set, while the fourth (fifth) condition, associated with the positive eigenvalue  $(-|v_n| + c)$ , propagates information from the boundary towards the flow region. It is consequently associated with a physical boundary condition (Figure 19.2.4).

The most appropriate physical condition, particularly for internal flows and corresponding to most experimental situations, consists in fixing the downstream static pressure. This can also be applied for external flow problems. However, in this latter case, free-stream velocity is generally imposed.

If the flow is supersonic normal to the inlet surface, all boundary conditions are physical.

With the same circumstances at the outlet, all eigenvalues are of negative sign and no physical conditions have to be given. All the boundary variables are defined by the interior flow, for instance via extrapolation formulas.

At a *solid wall boundary*, the normal velocity is zero, since no mass or other convective flux can penetrate the solid body. Hence, only one eigenvalue is positive and only one physical condition can be imposed, namely  $v_n = 0$ . The other variables at the wall, in particular velocity and pressure, have to be determined by extrapolation from the interior to the boundary (Figure 19.2.5).

An important effect of the numerical boundary procedure is to ensure that unwanted perturbations, generated in the computational domain, for instance the transients in a steady-state flow, leave the domain without being reflected at the boundaries. This implies that the propagation of these perturbations is compatible with the characteristic propagation properties of the Euler equations, as expressed by the compatibility relations or the equations for the characteristic variables.

When this is not the case, the accuracy of the computation can be greatly affected by the reflection occurring at the boundaries. It is therefore recommended to apply, as in the one-dimensional case, characteristic or compatibility relations as boundary procedures.

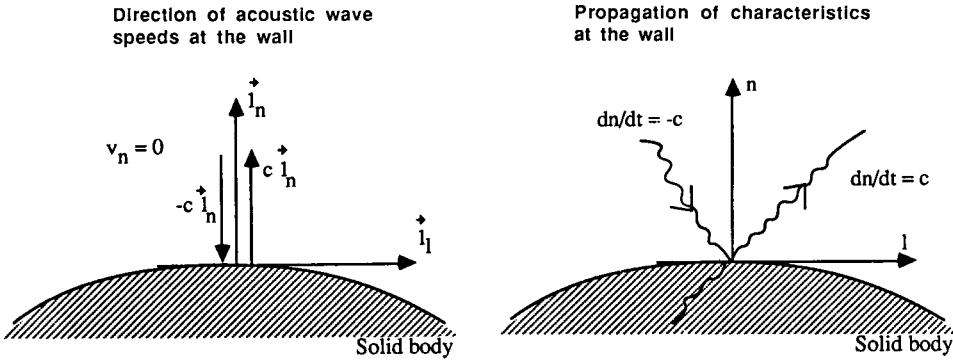


Figure 19.2.5 Solid wall boundary in two-dimensional flows

**19.2.2 Multi-dimensional compatibility relations**

The compatibility or characteristic relations can be written, for an arbitrary propagation direction, under the various formulations presented in Section 16.5.

They differ from their one-dimensional counterpart by the presence of contributions to the convective transport of characteristic quantities, arising from variations of velocity and pressure in the surface normal to the considered propagation direction. This is best seen in equation (16.5.46), which is the compatibility relation associated with the acoustic waves of celerity  $v_n \pm c$ .

This equation is reproduced here for the direction  $\vec{n}$  normal to the surface as

$$d_b^\pm R_n^\pm = \mp c \vec{l} \cdot (\vec{l} \cdot \vec{\nabla}) \vec{v} \tag{19.2.3}$$

where

$$d_b^\pm = \frac{\partial}{\partial t} + (\vec{v} \pm c \vec{l}_n) \cdot \vec{\nabla} \tag{19.2.4}$$

and with  $\vec{l}$  representing unit directions in the surface, that is normal to  $\vec{n}$ , namely

$$\vec{l} \cdot \vec{n} = 0 \tag{19.2.5}$$

The Riemann variables  $R_n^\pm$  associated with the direction  $n$  are defined by

$$R_n^\pm = \vec{v} \cdot \vec{l}_n \pm \frac{2c}{\gamma - 1} \tag{19.2.6}$$

as in the one-dimensional case.

It is seen here that these variables are generally not invariants, in the sense of being transported along an associated bicharacteristic, as a consequence of the presence of the right-hand side in equation (19.2.3).

The other characteristic relations are contained in the equations (16.5.51) to

(16.5.52) and are reproduced here for a two-dimensional flow and the direction  $\vec{n}$ :

$$\delta W = \begin{vmatrix} \delta w_1 \\ \delta w_2 \\ \delta w_3 \\ \delta w_4 \end{vmatrix} = \begin{vmatrix} \delta\rho - \frac{\delta p}{c^2} \\ \hat{n}_y \delta u - \hat{n}_x \delta v \\ \bar{\Gamma}_n \cdot \delta \vec{v} + \frac{\delta p}{\rho c} \\ -\bar{\Gamma}_n \cdot \delta \vec{v} + \frac{\delta p}{\rho c} \end{vmatrix} \quad (19.2.7)$$

The characteristic system becomes

$$\begin{aligned} \left( \frac{\partial}{\partial t} + \vec{v} \cdot \vec{\nabla} \right) w_1 &= 0 \\ \left( \frac{\partial}{\partial t} + \vec{v} \cdot \vec{\nabla} \right) w_2 &= \frac{c}{2} (\hat{n}_x \partial_y - \hat{n}_y \partial_x) (w_3 + w_4) = -\frac{1}{\rho} (\bar{\Gamma} \cdot \vec{\nabla}) p \\ \left[ \frac{\partial}{\partial t} + (\vec{v} + c \bar{\Gamma}_n) \cdot \vec{\nabla} \right] w_3 &= c (\hat{n}_x \partial_y - \hat{n}_y \partial_x) w_2 = -c \bar{\Gamma} \cdot (\bar{\Gamma} \cdot \vec{\nabla}) \vec{v} \\ \left[ \frac{\partial}{\partial t} + (\vec{v} - c \bar{\Gamma}_n) \cdot \vec{\nabla} \right] w_4 &= c (\hat{n}_x \partial_y - \hat{n}_y \partial_x) w_2 = -c \bar{\Gamma} \cdot (\bar{\Gamma} \cdot \vec{\nabla}) \vec{v} \end{aligned} \quad (19.2.8)$$

The first equation of (19.2.8) describes the constancy of entropy along a streamline, while the second characteristic equation has no equivalent in one-dimensional flows and represents the propagation of vorticity waves. The last two characteristic equations are identical to equation (19.2.3).

We recall here that these equations are to be considered as a shorthand form for the combination of primitive variable variations defined by (19.2.7) since, as pointed out in Chapter 16, the variables  $w$  cannot always be determined. However, if the flow is close to uniform, as in a far-field region of an immersed body, then the characteristic variables can be linearized around the uniform flow variables and  $W$  can always be defined, as seen in Chapter 16, Section 16.5.

If the *pressure and the velocity are uniform in the boundary surface*, that is

$$\bar{\Gamma} \cdot \vec{\nabla} p = 0 \quad \text{and} \quad (\bar{\Gamma} \cdot \vec{\nabla}) \vec{v} = 0 \quad (19.2.9)$$

then the right-hand sides of all the equations (19.2.8) vanish and one recovers locally a one-dimensional situation.

### 19.2.3 Far-field treatment for steady-state flows

A simple treatment of the inlet and outlet boundaries for stationary flows can be defined when (19.2.9) is valid (Thomas and Salas, 1986), where the

compatibility relations associated with the acoustic waves reduce to

$$R_n^+ = v_n + \frac{2c}{\gamma - 1} = \text{constant along the path } \vec{v} + c\vec{1}_n \quad (19.2.10)$$

$$R_n^- = v_n - \frac{2c}{\gamma - 1} = \text{constant along the path } \vec{v} - c\vec{1}_n \quad (19.2.11)$$

### *Subsonic inlet boundary*

The first relation corresponds to the positive, incoming, characteristic and is associated with the physical boundary condition. Hence, the values at the boundary, indicated by a subscript B, are obtained from

$$R_{nB}^+ = v_{nB} + \frac{2c_B}{\gamma - 1} = V_{n\infty} + \frac{2c_\infty}{\gamma - 1} \quad (19.2.12)$$

where  $\vec{V}_\infty$  is the free-stream velocity and  $c_\infty$  the free stream speed of sound.

The second relation (19.2.11) is associated with a numerical boundary condition and has to be estimated from inside the domain by an appropriate extrapolation from the mesh points close to the boundary surface. Hence,

$$R_{ni}^- = v_{nB} - \frac{2c_B}{\gamma - 1} = v_{ni} - \frac{2c_i}{\gamma - 1} \quad (19.2.13)$$

where the subscript i refers to a value at an internal mesh point along the direction  $\vec{v} - c\vec{1}_n$  or alternatively along the normal direction, since the boundary variations along the tangent to the surface have been assumed to vanish.

The boundary values of the normal velocity and sound speed are obtained by adding and subtracting equations (19.2.12) and (19.2.13), leading to

$$v_{nB} = \frac{R_{nB}^+ + R_{ni}^-}{2} \quad (19.2.14)$$

$$c_B = (R_{nB}^+ - R_{ni}^-) \frac{\gamma - 1}{4} \quad (19.2.15)$$

The second characteristic relation can be simplified if the local coordinate system is oriented such that the  $x$  direction is along the normal. In this case, the variable  $w_2$  reduces to the tangential velocity  $v_t$  and the compatibility relation becomes

$$\begin{aligned} v_t &= \text{constant along the directions } \vec{v} \text{ or } \vec{n} \\ s &= \text{constant along the direction } \vec{v} \text{ or } \vec{n} \end{aligned} \quad (19.2.16)$$

both variables being associated to the physical free-stream values; that is

$$v_{tB} = v_{t\infty} \quad (19.2.17)$$

$$s_B = s_\infty \quad (19.2.18)$$

The above treatment does not indicate that the stagnation enthalpy is constant and equal to its imposed value, since  $H$  is not associated with a characteristic variable. This is an extremely important aspect for steady calculations and should be enforced. This can be achieved in several ways, for instance by defining the speed of sound along the boundary by

$$c_B^2 = \left( \frac{H_\infty - \bar{v}_B^2}{2} \right) (\gamma - 1) \quad (19.2.19)$$

instead of equation (19.2.15).

Alternatively, one could replace equation (19.2.12) or (19.2.18) by the condition

$$H_B = H_\infty \quad (19.2.20)$$

### *Subsonic outlet boundary*

The same relations apply at the outlet, with the difference that the quantities  $R_{nB}^-$ ,  $v_{nB}$  and  $s_B$  are determined from the internal values. Remember that we define the direction of the normal towards the inside of the computational domain, that is  $v_n > 0$  at the inlet and  $v_n < 0$  at the outlet.

The fourth relation for  $R_{nB}^+$  is defined by the physical condition of fixed pressure:

$$R_{nB}^+ = -|v_{nB}| + \frac{2c_B}{\gamma - 1} = R_{n\infty}^+ = -|v_{n\infty}| + \frac{P_\infty}{\rho_\infty c_\infty} \quad (19.2.21)$$

If the flow is not uniform in the boundary surfaces the complete form (19.2.3) of the characteristic equations have to be used.

An equivalent formulation to the one just described can be defined by a direct extension of the treatment of Section 19.1.3 where the variables  $R_n^\pm$  are replaced by the characteristic variables  $\Delta w_3$  and  $\Delta w_4$ , while  $v_l$  and  $s$  are replaced by  $\Delta w_2$  and  $\Delta w_1$  respectively.

Also, the treatment of Chakravarthy, combining the time-differenced physical boundary conditions with the characteristic equations associated with the negative eigenvalues into one system of equations at the boundaries, can be extended in a straightforward way to two and three dimensions (Chakravarthy, 1983; Rai and Chaussee, 1983).

It is to be observed that other directions than the normal to the boundary surface may be selected in applying the characteristic relations. One interesting choice results from an analysis of Bayliss and Turkel (1982) which has been shown by Roe (1986) to correspond to a direction making an angle  $\theta$  with the incident velocity directions, supposed to be aligned with the  $x$  axis, such that  $\tan \theta = \beta^2 y / (x - \beta R M_\infty)$  with  $\beta^2 = 1 - M_\infty^2$  and  $R^2 = y^2 + x^2 / \beta^2$ .

### **19.2.4 Solid wall boundary**

At a solid wall one characteristic enters the flow domain and a single physical boundary condition is to be imposed. This condition is expressed by the

vanishing of the normal velocity

$$v_n = 0 \quad (19.2.22)$$

As a consequence, all convective flux components through the solid wall will vanish in the computation of the flux terms and the normal component of the flux vector reduces to the following expression in a two-dimensional flow:

$$\vec{F} \cdot \vec{1}_n = \begin{vmatrix} 0 \\ p\hat{n}_x \\ p\hat{n}_y \\ 0 \end{vmatrix} \quad (19.2.23)$$

Hence, only the pressure contribution remains at the walls.

The variables other than the normal velocity, in particular the tangential velocity, the pressure and another thermodynamic variables, for instance total enthalpy or entropy, have to be obtained from the interior flow. Here again these variables can be extrapolated directly from their values at points adjacent to the wall surface, or the conservation equations can be solved for mesh points on the boundary from a one-sided discretization.

A third alternative consists in applying the characteristic relations discretized in a one-sided way from the wall towards the inside of the flow field. It is essential to observe here that the simplified form of the compatibility relations, namely equations (19.2.10), (19.2.11) and (19.2.16), are not valid here, since the assumption of uniform velocity and pressure in the boundary surface is certainly not satisfied at a solid wall boundary. Hence the full form (19.2.7) and (19.2.8) has to be applied at the walls.

These relations are applied in differential form in the combined treatment of Chakravarthy, where the equation for  $w_3$ , associated with a positive characteristic, is replaced by the time-differenced form of the physical boundary condition (19.2.22) (Chakravarthy, 1983; Rai and Chaussee, 1983).

#### *Determination of the wall pressure*

The numerical determination of the wall pressure is an essential element in any computation with solid boundaries and various methods can be applied in order to obtain the wall pressures.

*Extrapolation from adjacent points* This is the simplest approach, whereby an extrapolation, generally linear or quadratic, is applied from neighbouring points to the wall along a mesh point line.

When mesh points are located on the wall, as in Figure 19.2.6, one can also solve the Euler equations with one-sided discretizations to find all the variables in addition to the vanishing normal velocity.

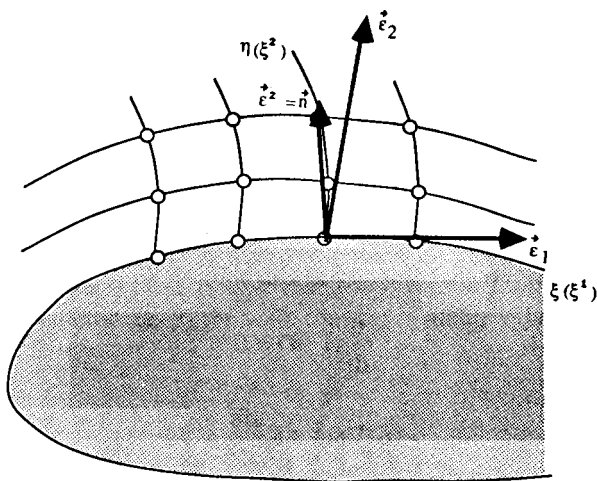


Figure 19.2.6 Streamwise curvilinear coordinates at solid boundary

**Compatibility relations at the wall** The wall pressure can be obtained from a one-sided discretization of the compatibility relations (19.2.8), considered as a system where the equation for  $w_3$  is replaced by the physical boundary condition.

These equations couple streamwise and normal derivatives of the pressure, for instance the equation for  $w_4$  becomes at the solid wall

$$-\frac{1}{\rho c} \frac{\partial p}{\partial t} - \frac{1}{R_w} v_l^2 - \frac{v_l}{\rho c} \frac{\partial p}{\partial l} + \frac{1}{\rho} \frac{\partial p}{\partial n} = c \bar{\nabla} \cdot \bar{v} \quad (19.2.24)$$

where  $R_w$  is the wall radius of curvature and  $\partial l$  is the elementary arc length along the wall. If the continuity equation is subtracted from equation (19.2.24), after having replaced the density variations by the isentropic pressure variations, that is under the form

$$\frac{1}{\rho c} \frac{\partial p}{\partial t} + c \bar{\nabla} \cdot \bar{v} + \frac{\bar{v}}{\rho c} \cdot \bar{\nabla} p = 0 \quad (19.2.25)$$

one is left with the following equation, which is nothing else than the normal projection of the momentum equation at the wall:

$$\frac{1}{R_w} v_l^2 = \frac{1}{\rho} \frac{\partial p}{\partial n} \quad (19.2.26)$$

Hence a third way, recommended initially by Rizzi (1978), consists in discretizing directly the normal momentum equation at the wall.

**Normal momentum equation** Equation (19.2.26) is discretized in a one-sided way along the normal to the solid wall boundary.

In practical computations, however, one has seldom a mesh system formed by normals to the wall, that is mesh points aligned along the wall normals. Consequently, equation (19.2.26) is difficult to discretize as it stands and a more appropriate form is based on the projection of the momentum equation in arbitrary curvilinear coordinates,  $(\xi, \eta)$  in two dimensions, with the coordinate line  $\eta = \text{constant}$  being the wall surface (Figure 19.2.6).

Projecting the momentum equation along the normal to the wall corresponds to taking the second contravariant component, if one defines  $\xi = \xi^1$  and  $\eta = \xi^2$ . From the vanishing normal velocity at the wall,

$$\frac{d}{dt}(\vec{v} \cdot \vec{n}) = 0 \tag{19.2.27a}$$

one has

$$-\vec{n} \cdot \vec{\nabla} p + \rho \vec{v} \cdot \frac{d\vec{n}}{dt} = 0 \tag{19.2.27b}$$

For stationary walls, the second term reduces to the streamwise derivative

$$-\vec{n} \cdot \vec{\nabla} p + \rho \vec{v} \cdot (\vec{v} \cdot \vec{\nabla}) \vec{n} = 0 \tag{19.2.28}$$

With  $\vec{n}$  equal to the unit vector  $\vec{1}_n$  along the normal, this equation leads directly to equation (19.2.26).

Taking  $\vec{n} = \vec{e}^{-2} = \vec{\nabla} \eta$  leads to

$$\begin{aligned} \vec{e}^{-2} \cdot \vec{\nabla} p &= \frac{\partial p}{\partial n} \sqrt{\eta_x^2 + \eta_y^2} \\ &= g^{2a} \partial_a p = (\xi_x \eta_x + \xi_y \eta_y) \frac{\partial p}{\partial \xi} + (\eta_x^2 + \eta_y^2) \frac{\partial p}{\partial \eta} \\ &= \rho \vec{v} \cdot (\vec{v} \cdot \vec{\nabla}) \vec{n} = -\rho \vec{n} \cdot (\vec{v} \cdot \vec{\nabla}) \vec{v} \\ &= -\rho \vec{U} \vec{n} \cdot \frac{\partial \vec{v}}{\partial \xi} = -\rho \vec{U} \left( \eta_x \frac{\partial u}{\partial \xi} + \eta_y \frac{\partial v}{\partial \xi} \right) \end{aligned} \tag{19.2.29}$$

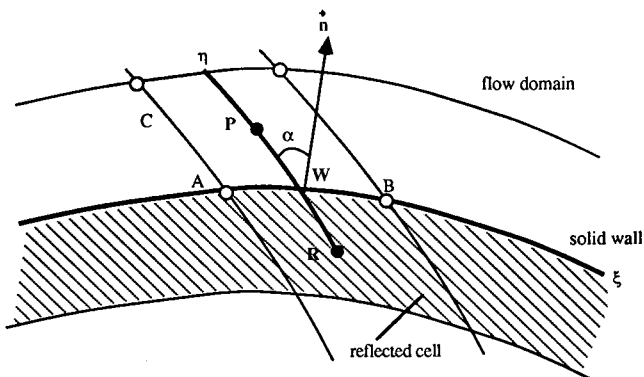


Figure 19.2.7 Reflected boundary cell at a solid boundary

The contravariant  $\xi$  component  $\tilde{U}$  of the velocity vector is defined by

$$\tilde{U} = \xi_x u + \xi_y v \quad (19.2.30)$$

where the subscripts on  $\xi$  and  $\eta$  indicate partial derivatives. This formula can be applied to estimate  $\partial p / \partial n$  by calculating the metric coefficients from the mesh point coordinates. Note that alternative expressions can also be obtained from these equations (see Problem 19.20).

A current implementation technique is based on the definition of reflected cells as shown in Figure 19.2.7, where the flow variables are defined as to ensure vanishing normal velocities at the wall; that is one defines the conditions at the reflected point R by

$$\begin{aligned} \rho_R &= \rho_P \\ v_{IR} &= v_{IP} \\ v_{nR} &= -v_{nP} \\ p_R &= p_P - \left( \frac{\partial p}{\partial \eta} \right)_w \Delta \eta_{RP} \end{aligned} \quad (19.2.31)$$

The derivative in the direction of the curvilinear coordinate  $\eta$  is related to the normal pressure gradient by relations (19.2.29). The derivative  $\partial p / \partial \eta$  is estimated at the wall and the wall values of all the variables are obtained from the arithmetic average between P and R. Hence,

$$p_w = \frac{p_P + p_R}{2} = p_P - \frac{1}{2} \left( \frac{\partial p}{\partial \eta} \right)_w \Delta \eta_{RP} \quad (19.2.32a)$$

If the radius of curvature is known,  $\partial p / \partial n$  is given by equation (19.2.26) and  $\partial p / \partial \eta$  is estimated directly from

$$\frac{\partial p}{\partial n} = \frac{\partial p}{\partial \eta} \left( \frac{\partial \eta}{\partial n} \right) + \frac{\partial p}{\partial \xi} \left( \frac{\partial \xi}{\partial n} \right) = \frac{\partial p}{\partial \eta} \frac{1}{\cos \alpha} + \frac{\partial p}{\partial \xi} \tan \alpha \quad (19.2.32b)$$

where the angle  $\alpha$  is obtained from  $\cos \alpha = (\text{area of cell}) / (AB \cdot AC)$  and  $\partial p / \partial \xi$  can be approximated with a central finite difference of  $p$  along the solid wall.

A further improvement is obtained by the replacement of the second reflection condition on the tangential velocity at the wall by the condition of vanishing wall vorticity if the flow conditions are irrotational. In this case, the discretization of the following equation leads to an alternative to the third equation (19.2.31)

$$\frac{\partial v_t}{\partial n} + \frac{v_t}{R_w} = 0 \quad (19.2.33)$$

The normal derivative of the tangential velocity is estimated from the chain rule as in equation (19.2.32b). If the  $\eta$  direction is normal to  $\xi$ , equation (19.2.33) can be approximated as follows:

$$\frac{v_{IP} - v_{IR}}{\Delta \eta_{RP}} + \frac{v_{IP} + v_{IR}}{2R_w} = 0 \quad (19.2.34)$$

from which the tangential velocity in the reflected cell  $v_{IR}$  can be estimated, leading to

$$v_{IR} = v_{IP} \frac{1 + \Delta\eta_{RP}/R_w}{1 - \Delta\eta_{RP}/R_w} \quad (19.2.35)$$

### 19.2.5 Non-reflective boundary conditions

As in one dimension, non-reflective boundary conditions can be imposed as physical boundary conditions in order to prevent the outgoing waves from producing unwanted reflections at the boundaries.

Referring to the characteristic equations (19.2.7) and (19.2.8), written in the condensed form

$$\frac{\partial w_k}{\partial t} + (\bar{a}_k \cdot \bar{V}) w_k = b_k \quad k = 1, \dots, 4 \quad (19.2.36)$$

where  $b_k$  represents the right-hand side of equations (19.2.8) and  $\bar{a}_k = \lambda_k \bar{I}_n$ .

For all characteristics corresponding to incoming waves in the direction normal to the boundary, that is with positive eigenvalues  $\lambda$ , the non-reflective boundary condition becomes

$$\frac{\partial w_k}{\partial t} = b_k \quad \text{for all } \lambda_k > 0 \quad (19.2.37)$$

For instance, at a subsonic outlet section where  $\lambda_4 > 0$ , this condition is written as

$$\bar{I}_n \cdot \frac{\partial \bar{v}}{\partial t} - \frac{1}{\rho c} \frac{\partial p}{\partial t} = c \frac{\partial v_t}{\partial l} \quad (19.2.38)$$

where the right-hand side represents the tangential variations of the velocity components in the boundary surface. When these variations are zero, either for uniform conditions in the exit surface or for normal exit velocities, then condition (19.2.38) is identical locally to the one-dimensional form.

The adaptation of Rudy and Strickwerda (1980) can be applied in the following form, instead of (19.2.38) for an imposed exit pressure  $p^*$ :

$$\frac{\partial v_n}{\partial t} - \frac{1}{\rho c} \frac{\partial p}{\partial t} - \frac{\alpha}{\rho c} (p - p^*) = c \frac{\partial v_t}{\partial l} \quad (19.2.39)$$

where  $\alpha > 0$  has to be calibrated empirically.

### 19.3 THE FAR-FIELD BOUNDARY CORRECTIONS

In external as well as internal flow problems the inlet and outlet boundaries are assumed to be located far enough from the main flow region so that the influence of the flow disturbances does not affect the free-stream values.

Since these disturbances generally require long distances to damp out, the boundaries will have to be situated, in practice, at an appreciable distance from the source of the disturbances, for instance an airfoil in an external flow problem. In this latter case, a distance of the order of or larger than 50 chords between the airfoil and the far-field boundary is not uncommon.

These large distances have to be filled either with a very large number of mesh points in the far-field region, where on the other hand the flow variations are often unimportant, or with very large mesh cells having reduced accuracy. Both situations are undesirable and could be overcome if an approximate behaviour of the far-field flow would be known and matched to the interior flow field by an adaptation of the boundary conditions. As a consequence, the external boundaries could be taken closer to the disturbed flow region with a reduction in the total number of mesh points, reducing the total computational cost while improving the accuracy.

An approximate description of the far field can easily be obtained by introducing a perturbation field to the uniform flow and expressing it as an asymptotic series in a perturbation parameter. In the inviscid far field, the perturbation satisfies the small disturbance potential equation

$$(1 - M_\infty^2)\phi'_{x'x'} + \phi'_{y'y'} = 0 \quad (19.3.1)$$

where  $x'$  and  $y'$  are directions along and normal to the free-stream velocity and  $M_\infty$  the associated Mach number. The potential  $\phi'$  is the isentropic disturbance field defining the perturbation velocities as

$$\bar{v}' = \bar{\nabla}\phi' \quad (19.3.2)$$

A solution can be obtained as a series expansion in function of  $x'$  and  $y'$ , or of corresponding polar coordinates. For external flow problems, a solution can be found of the form (see, for instance, Thomas and Salas, 1986)

$$\begin{aligned} u' &= \sum_{k=1}^{\infty} \frac{1}{r^k} [b'_k \cos(k\theta) + c'_k \sin(k\theta)] \\ v' &= \sum_{k=1}^{\infty} \frac{1}{r^k} [b'_k \sin(k\theta) + c'_k \cos(k\theta)] \end{aligned} \quad (19.3.3)$$

where  $r$  is the radius measured from the quarter chord of the airfoil and  $\theta$  the polar angle. The coefficients can be obtained numerically by matching this expansion to the numerical solution along a boundary at a certain distance from the airfoil, such as the surface  $S_1$  on Figure 19.3.1.

In the case of an isolated airfoil, however, theoretical far-field expansions can

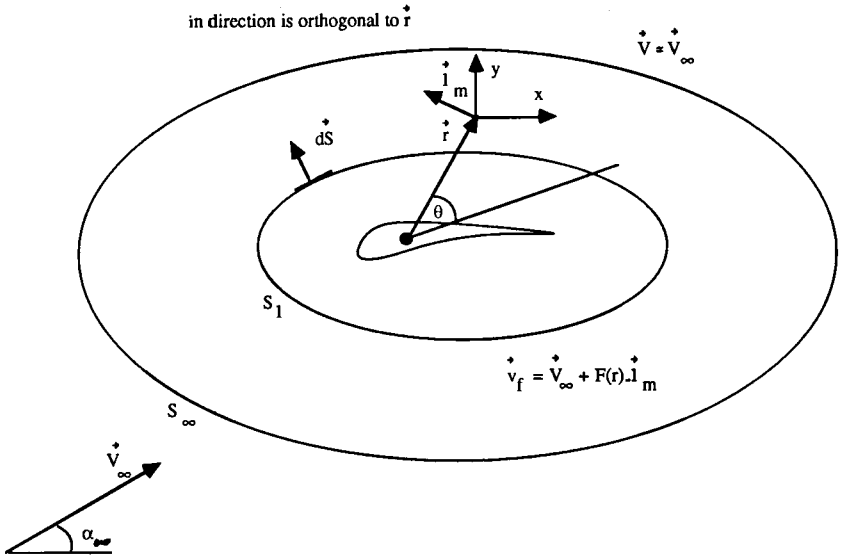


Figure 19.3.1 Far-field boundaries for flow along airfoil

be derived for thin airfoils, where the  $b'$  coefficients are related to the thickness distribution and the  $c'$  coefficients to the circulation.

To the lowest order one obtains the corrections  $u_f$  and  $v_f$  to the far-field velocities, expressed as fractions of the free-stream velocity  $\vec{V}_\infty$ , under an incidence angle of  $\alpha_\infty$ :

$$\frac{u_f}{|\vec{V}_\infty|} = \cos \alpha_\infty + F \sin \theta$$

$$\frac{v_f}{|\vec{V}_\infty|} = \sin \alpha_\infty - F \cos \theta$$
(19.3.4)

where  $F$  is defined as a function of the circulation  $\Gamma$  by

$$F = \frac{\Gamma}{|\vec{V}_\infty|} \frac{\beta}{2\pi r} \frac{1}{1 - M_\infty^2 \sin^2(\theta - \alpha_\infty)}$$
(19.3.5)

with

$$\beta = \sqrt{1 - M_\infty^2}$$
(19.3.6)

The circulation  $\Gamma$  is obtained from the lift coefficient

$$C_L = \frac{2\Gamma}{|\vec{V}_\infty|c}$$
(19.3.7)

for an airfoil with chord  $c$ , where the lift coefficient is calculated from a momentum flux balance over an arbitrary closed contour  $S$  around the airfoil.

The axial and normal forces  $L_x$  and  $L_y$ , expressed as coefficients, normalized by the free-stream dynamic pressure and the chord  $c$ , are calculated from the

following momentum balance (see, for instance, Yu *et al.*, 1983, for an overview of drag and lift calculations):

$$C_x = \frac{2L_x}{\rho_\infty(U_\infty^2 + V_\infty^2)c} = \frac{-2}{\rho_\infty(U_\infty^2 + V_\infty^2)c} \oint_S [\rho u(\vec{v} \cdot d\vec{S}) + p \vec{1}_x \cdot d\vec{S}] \quad (19.3.8)$$

$$C_y = \frac{2L_y}{\rho_\infty(U_\infty^2 + V_\infty^2)c} = \frac{-2}{\rho_\infty(U_\infty^2 + V_\infty^2)c} \oint_S [\rho v(\vec{v} \cdot d\vec{S}) + p \vec{1}_y \cdot d\vec{S}] \quad (19.3.9)$$

The corrected far-field velocities are to be introduced in the boundary conditions, replacing the velocities with the subscript B in the relations of Section 19.2.2.

The application of this correction leads to an improvement in the accuracy and allows the far-field boundary to be placed at distances of the order of five chords without penalty on the accuracy. An example, from Pulliam and Steger (1985), shows the variation of lift coefficient with the outer distance of the boundaries for an NACA 0012 airfoil at subsonic incidence conditions.

Figure 19.3.2 compares the variation of the lift coefficient with and without the far-field corrections, (19.3.4) to (19.3.6), demonstrating the spectacular improvement.

A more general formulation, valid for external and internal flows, has been developed by Gustafsson (1982), Ferm and Gustafsson (1982), Gustafsson and Ferm (1986), Verhoff (1985), Hirsch and Verhoff (1989). In this approach the Euler equations are linearized in the far field and analytical solutions are obtained for the perturbations from the uniform conditions at infinity, as a Fourier series expansion in the direction along the boundary, allowing also far field perturbations for the entropy waves. The coefficients of the expansion are written in the form of exponentials in the incoming direction, normal to the boundary. The linearized form of the compatibility equations (19.2.8) can be written as follows

$$\frac{\partial w'_1}{\partial \tau} + M_\infty \frac{\partial w'_1}{\partial x} = 0 \quad (19.3.10a)$$

$$\frac{\partial w'_2}{\partial \tau} + M_\infty \frac{\partial w'_2}{\partial x} + \frac{1}{2} \frac{\partial (w'_3 + w'_4)}{\partial y} = 0 \quad (19.3.10b)$$

$$\frac{\partial w'_3}{\partial \tau} + (M_\infty + 1) \frac{\partial w'_3}{\partial x} + \frac{\partial w'_2}{\partial y} = 0 \quad (19.3.10c)$$

$$\frac{\partial w'_4}{\partial \tau} + (M_\infty - 1) \frac{\partial w'_4}{\partial x} + \frac{\partial w'_2}{\partial y} = 0 \quad (19.3.10d)$$

where the dash indicates perturbations from the free stream values.

Considering the internal nozzle flow of Figure 19.3.3, an expansion of the form

$$w'_2 = \sum_{m=1}^{\infty} h_m(x) \sin \frac{m\pi y}{b} \quad (19.3.11a)$$

$$w'_3 = \sum_{m=1}^{\infty} f_m(x) \cos \frac{m\pi y}{b} \quad (19.3.11b)$$

$$w'_4 = \sum_{m=1}^{\infty} g_m(x) \cos \frac{m\pi y}{b} \quad (19.3.11c)$$

is considered.

Since the first characteristic variable, which is proportional to the entropy, is purely convected and decoupled from the other equations, we can solve separately for the entropy perturbation and remove the corresponding equation from the system (19.3.10).

The choice of the Fourier terms results from the flow tangency boundary condition at the solid walls  $y = \pm b/2$ . Introducing these solutions in the stationary form of equations (19.3.10) leads to the following system, for an arbitrary Fourier mode  $m$ , writing  $M$  instead of  $M_{\infty}$ , the free stream Mach number and removing the subscript  $m$  on the amplitudes  $f$ ,  $g$  and  $h$ .

$$\begin{aligned} (M+1) \frac{\partial f}{\partial x} + \frac{m\pi}{b} h &= 0 \\ (M-1) \frac{\partial g}{\partial x} + \frac{m\pi}{b} h &= 0 \\ M \frac{\partial h}{\partial x} - \frac{m\pi}{2b} (f+g) &= 0 \end{aligned} \quad (19.3.12)$$

For each Fourier mode, solutions of the form

$$\begin{vmatrix} f \\ g \\ h \end{vmatrix} = \begin{vmatrix} f \\ g \\ h \end{vmatrix}_0 e^{-\mu x} \quad (19.3.13)$$

can be applied in the inflow region, with  $x$  measured from the boundary on. The coefficients  $\mu$  are eigenvalues of the system (19.3.12) and the amplitudes are proportional to the eigenvectors of this system. The general solution is of the form

$$\begin{vmatrix} f \\ g \\ h \end{vmatrix} = C_1 \begin{vmatrix} 1 \\ -1 \\ 0 \end{vmatrix} + C_2 \begin{vmatrix} \beta \\ M+1 \\ -\beta \\ 1-M \\ 1 \end{vmatrix} e^{-(m\pi/b\beta)x} + C_3 \begin{vmatrix} -\beta \\ M+1 \\ \beta \\ 1-M \\ 1 \end{vmatrix} e^{(m\pi/b\beta)x} \quad (19.3.14)$$

From the properties of the characteristic variables it is known that  $w'_2$  and  $w'_3$  are characteristics propagating from left to right (for positive  $u$ ), while  $w'_4$  is propagating right to left for a subsonic flow, since they correspond respectively to wave speeds  $u$ ,  $u + c$  and  $u - c$ . Hence, in order to determine the far field disturbances we express the amplitudes of the incoming characteristic perturbations as zero at infinity, **leading to a correction on the physical boundary conditions for finite distances**, and the amplitudes of the outgoing characteristics are defined by the numerical solution at the boundary.

Hence, for the variables associated with the outgoing waves, a relation is obtained for the coefficients  $C$  by developing the numerically obtained internal solution at the boundary  $AA$  ( $x = 0$ ), for instance, as a Fourier series in  $y$ .

Figure 19.3.4 shows an example, from Verhoff (1985), of a two dimensional nozzle flow comparing the computed solutions on the boundaries and in the constant area regions, with and without the far-field matching procedure.

The figures compare the Mach number distributions for the nozzle mesh shown in Figure 19.3.4 (a), when boundary conditions are applied at the sections  $AA$  and  $BB$  (solid line) or at the limits of the computational domain (dashed line).

Figure 19.3.4 (b) is obtained with characteristic-type boundary conditions, while Figure 19.3.4 (c) applies the perturbation expansion. As can be seen, the error introduced by applying these boundary conditions in sections  $AA$  and  $BB$  is very small, demonstrating the effectiveness of adapted far field corrections.

Another example is shown in the following figures for the transonic flow through a similar nozzle, demonstrating the validity of this boundary treatment for non-isentropic flows. Figure 19.3.5 shows the isoMach number distributions in the central part of the long channel, with the presence of a curved shock, resulting in a non uniform entropy downstream of the shock, comparing the results obtained for the extended and restricted domains, the latter with uncorrected (b) and corrected (c) boundary treatment.

The Mach number distributions on the lower and upper walls are shown on Figure 19.3.6, for the three cases of Figure 19.3.5. There is a shift in the shock position by one mesh cell, which is not very significant even on this relatively coarse mesh. The improvement due to the boundary corrections is clearly seen. Another measure of the corrections concerns the inlet angles; the corrected inlet angle for the short channel is 2.6 degrees, to be compared with the value of 2.7 degrees calculated along the same section of the long channel, while in the uncorrected case the inlet angle is fixed at zero degrees. Another display of the effects of the boundary treatment is shown on Figure 19.3.7 where the Mach number profiles are compared at inlet and outlet of the short channel. The differences between the dashed lines and the plus-symbols indicate the amplitude of the corrections on the short channel, while the solid line is the reference value from the long channel. The small difference between the latter and the corrected values of the short channel computation (+ symbols) is probably due to the fact that the boundaries of the long channel have not been taken far enough. This confirms again the efficiency of this boundary treatment.

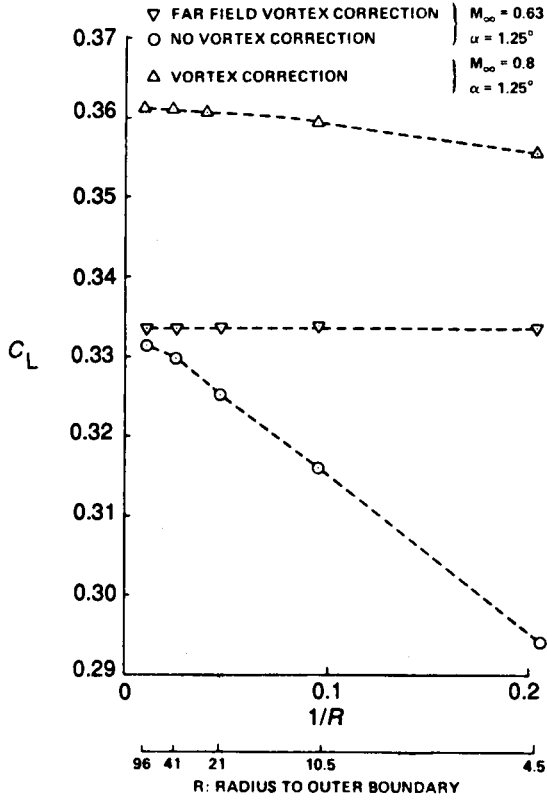


**Figure 19.3.2** Effect on lift of varying outer boundary distances with and without vortex correction. (From Pulliam and Steger, 1985)

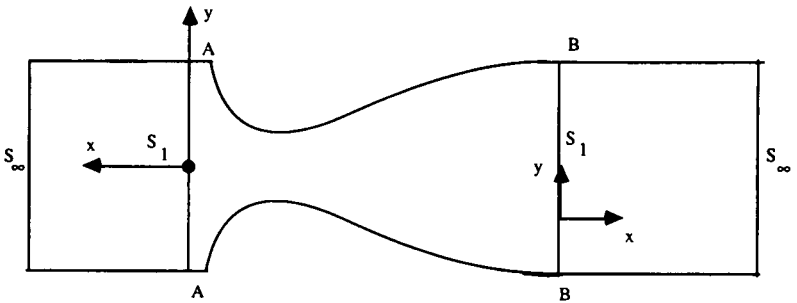
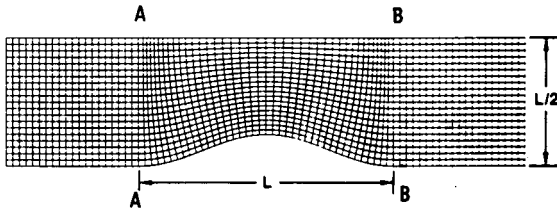
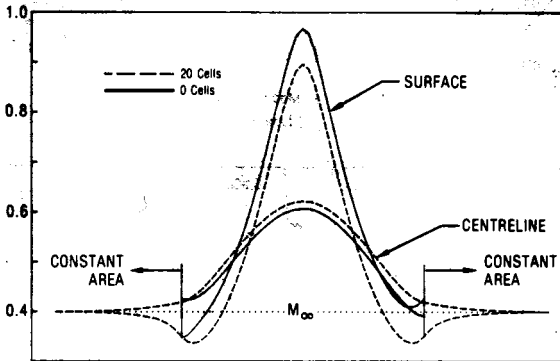


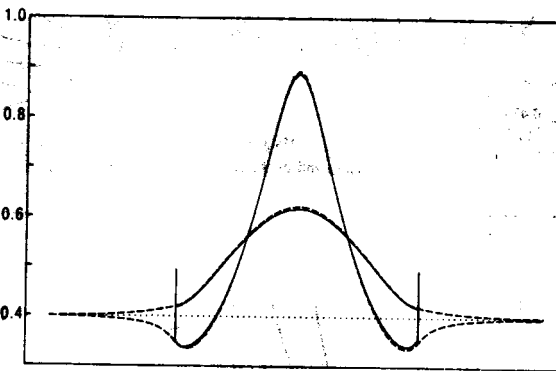
**Figure 19.3.3** Far-field regions for nozzle flow. The regions left of AA and right of BB are considered as far field



(a) Nozzle geometry and grid



(b) Mach numbers distribution obtained with characteristic - type boundary conditions. Solid line : boundaries in AA, BB



(c) Mach number distribution obtained with perturbation boundary conditions. Solid line : boundaries in AA, BB

**Figure 19.3.4** Comparison of characteristic and perturbation boundary conditions. (Courtesy A. Verhoff, McDonnell Aircraft Co., USA)

Therefore we suggest applying and deriving perturbative far field corrections whenever possible. It always reduces considerably the extension of the computational domain, while maintaining the required accuracy.

Applications of the Fourier series development of the flow disturbances along

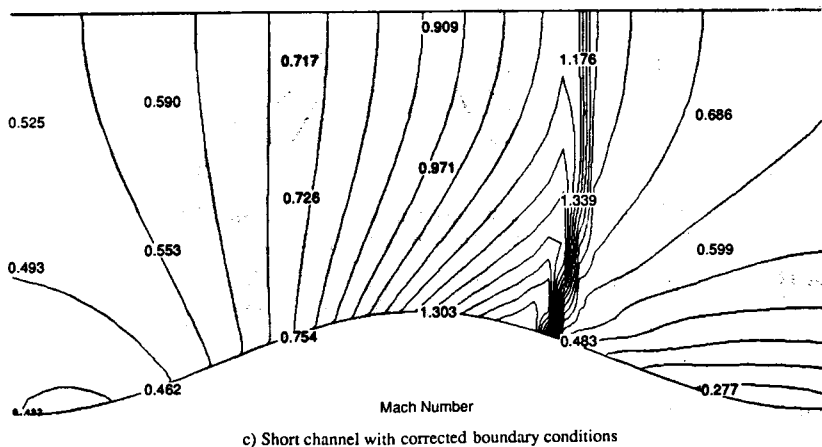
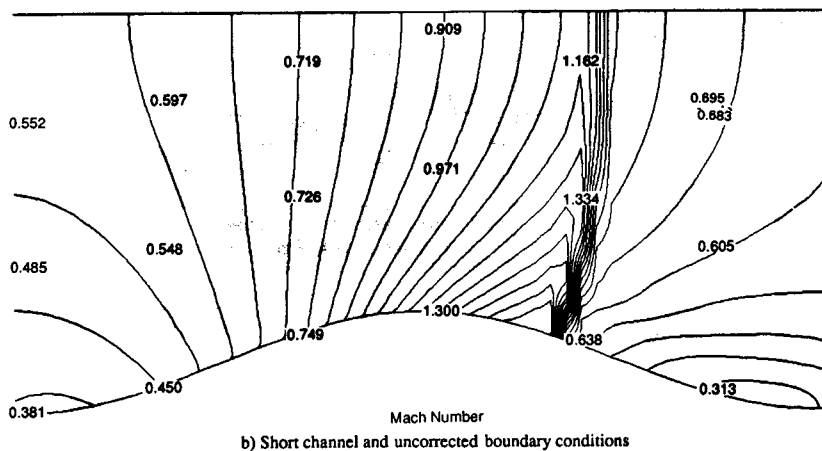
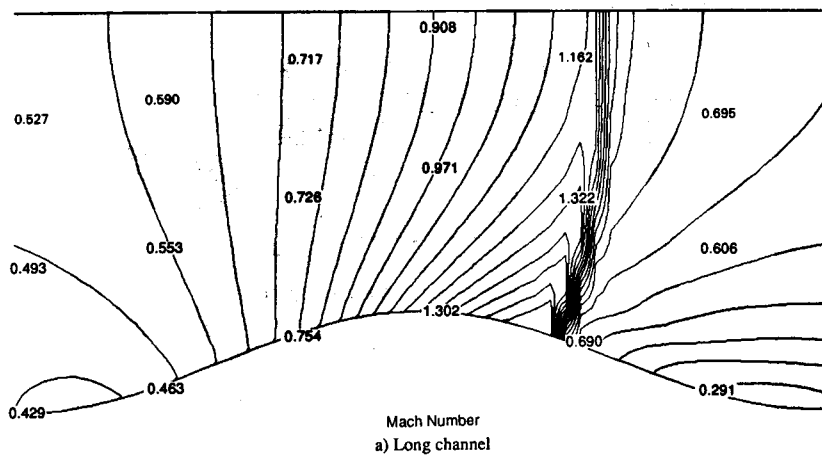


**Figure 19.3.5** Comparison of iso-Mach lines in the central part of the sinusoidal channel at transonic conditions

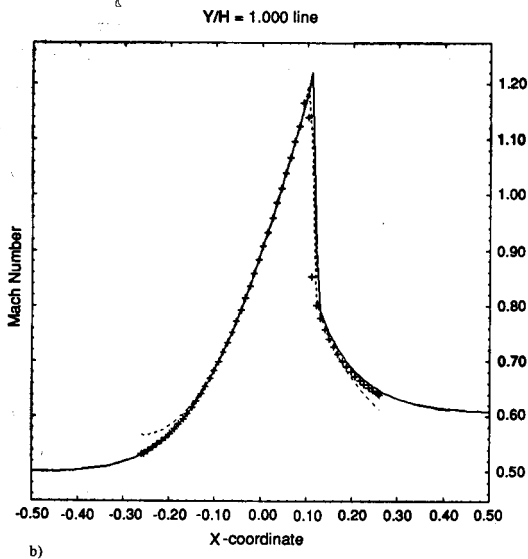
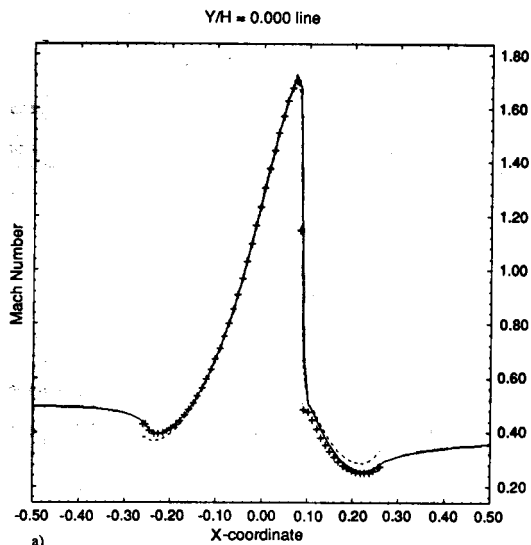


**Figure 19.3.6** Comparison of Mach number distributions in the central part of the sinusoidal channel at transonic conditions on lower (a) and upper (b) walls  
 Solid line: long channel  
 Dashed line: short channel and uncorrected boundary conditions  
 ++ symbols: short channel with corrected boundary conditions

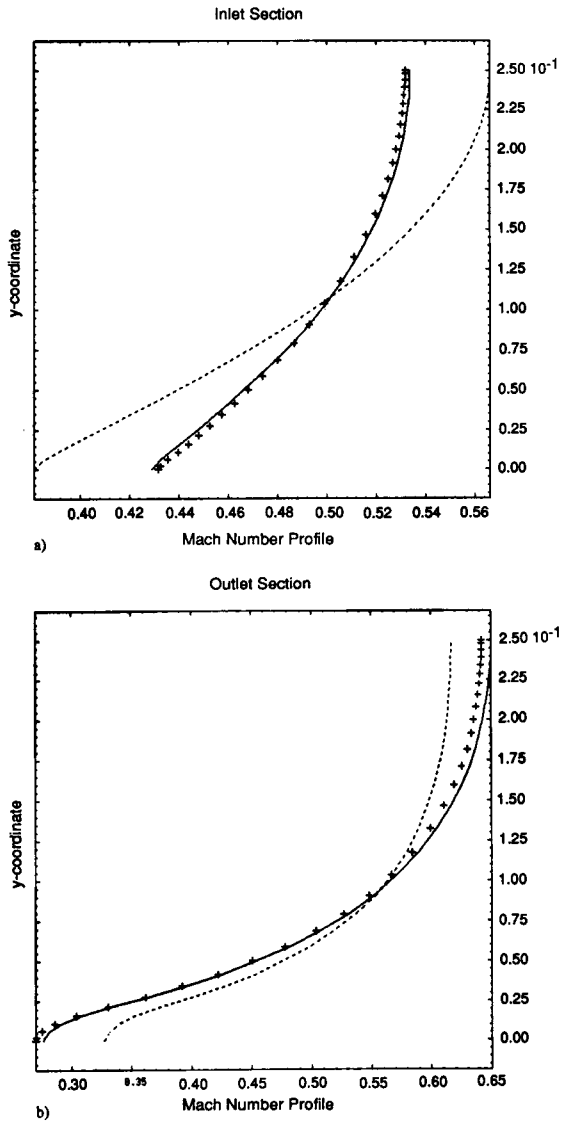


**Figure 19.3.7** Comparison of Mach number distributions along the inlet (a) and exit (b) stations of the short sinusoidal channel at transonic conditions  
 Solid line: long channel  
 Dashed line: short channel and uncorrected boundary conditions  
 ++ symbols: short channel with corrected boundary conditions

the boundaries have also been applied by Giles (1988), (1989) within the context of non-reflective boundary conditions.

It is of interest to notice the differences between the non-reflective boundary conditions and the far field corrections obtained by the above approach. Although the basic idea remains the same, namely to avoid incoming disturbances, the former approach expresses this condition at the finite distance location of the computational boundary, while the latter approach expresses this condition at infinity. From this requirement, an exact linearized solution is obtained in the far field. Hence the far field corrections give rise to incoming disturbances at finite distances which tend to zero at infinity. This is the correct physical assumption while the non-reflective conditions are approximations when expressed at finite distances.

However, linearized exact solutions cannot always be easily obtained and in these cases the application of non-reflective conditions at finite distances is the next best approximation.

#### 19.4 THE KUTTA CONDITION

It is well known that inviscid flows over lifting bodies, such as airfoils, have an infinity of solutions depending on a free parameter, namely the circulation around the airfoil.

The Kutta condition states that the closest approximation to the physical, viscous reality is obtained for the value of the circulation which locates the downstream stagnation point at the sharp trailing edge of the airfoil.

This condition, which can be implemented in a variety of ways, is essential in potential flows in order to compute lifting airfoils. As seen in Chapter 13, a jump in potential equal to the circulation has to be introduced along a cut in the computational domain, simulating a singularity-vortex sheet. The intensity of the potential discontinuity is determined, for instance, by imposing equal pressures or velocities at the trailing edge points on the pressure and suction surfaces.

At a Workshop on inviscid transonic flow computations (Rizzi and Viviani, 1981), it appeared that computations based on the Euler equations, and which did not implement any form of Kutta condition, still produced accurate results, with the correct value of the circulation.

This has been confirmed since then by many computations on two-dimensional as well as three-dimensional airfoils and wings; see, for instance, Rizzi (1982, 1985).

It seems, therefore, that it is not necessary to impose a Kutta condition on calculations with time-dependent Euler flow models in order to obtain the correct lift on airfoils with sharp trailing edges. This remarkable result implies

the existence of some mechanism in the pseudo-time evolution of the computed Euler solutions, which reproduces and simulates the essential physical phenomena leading to the generation of circulation and lift.

It is well known (see, for instance, Prandtl, 1952, pp. 50–52, 69–70; Batchelor, 1970) that this mechanism is of a transient nature and is induced by the presence of an eddy at the trailing edge, generating a surface of discontinuity in the inviscid flow. In a viscous flow this surface of discontinuity will diffuse into a thin shear layer and form the wake of the airfoil.

Indeed, at the initial instants the flow behaves in an irrotational manner with a stagnation point *S* on the suction surface inducing a turning of the flow around the sharp trailing edge (Figure 19.4.1(a)).

Around the trailing edge, very strong velocity gradients exist since the inviscid, incompressible velocity tends to infinity at *P* and the compressible flow will expand up to zero vacuum pressure. By some mechanism, an eddy is formed at *P*, preventing the infinite velocities or the vacuum conditions, and a surface of discontinuity appears, also called a vortex sheet, along which the two flows from the pressure and suction sides merge with a discontinuity in the tangential velocity (Figure 19.4.1(b)).

Note that the generation of this surface of discontinuity is not in contradiction with Kelvin's theorems on the impossibility of vorticity creation in inviscid flows, since there are no streamlines that join points on the two sides of the surface of discontinuity. Therefore this surface is a possible weak solution of the Euler equations, in the same way as shocks.

The counterclockwise velocity induced by the eddy on the suction surface moves the stagnation point *S* towards the trailing edge *P*. As long as the stagnation point remains on the upper airfoil side, the discontinuity surface rolls up and feeds the eddy intensity, increasing the induced velocity which tends to move *S* towards *P*. After some short time, the stagnation point has indeed reached the trailing edge and the eddy is transported by convection downstream of the airfoil (Figure 19.4.1(c)).

Finally, a circulation appears around the airfoil, equal and opposite to the circulation around the downstream convected eddy (Figure 19.4.1(d)) such that the total circulation around any contour enclosing the airfoil and the rolling-up eddy is zero according to Kelvin's theorem.

This sequence of events can not be simulated with potential flows, since this isentropic, irrotational flow model does not allow for vortex sheets with a discontinuity in tangential velocities.

With the Euler flow model, on the other hand, vortex sheets can be captured by the computations and this transient sequence of events can be simulated numerically and inviscidly as soon as some mechanism exists that would trigger the generation of the trailing edge eddy of Figure 19.4.1(b).

Prandtl (1952) does not specify by which mechanism a trailing edge eddy can be produced, but it is clear from his remarks (pp. 51 and 58) that viscosity plays

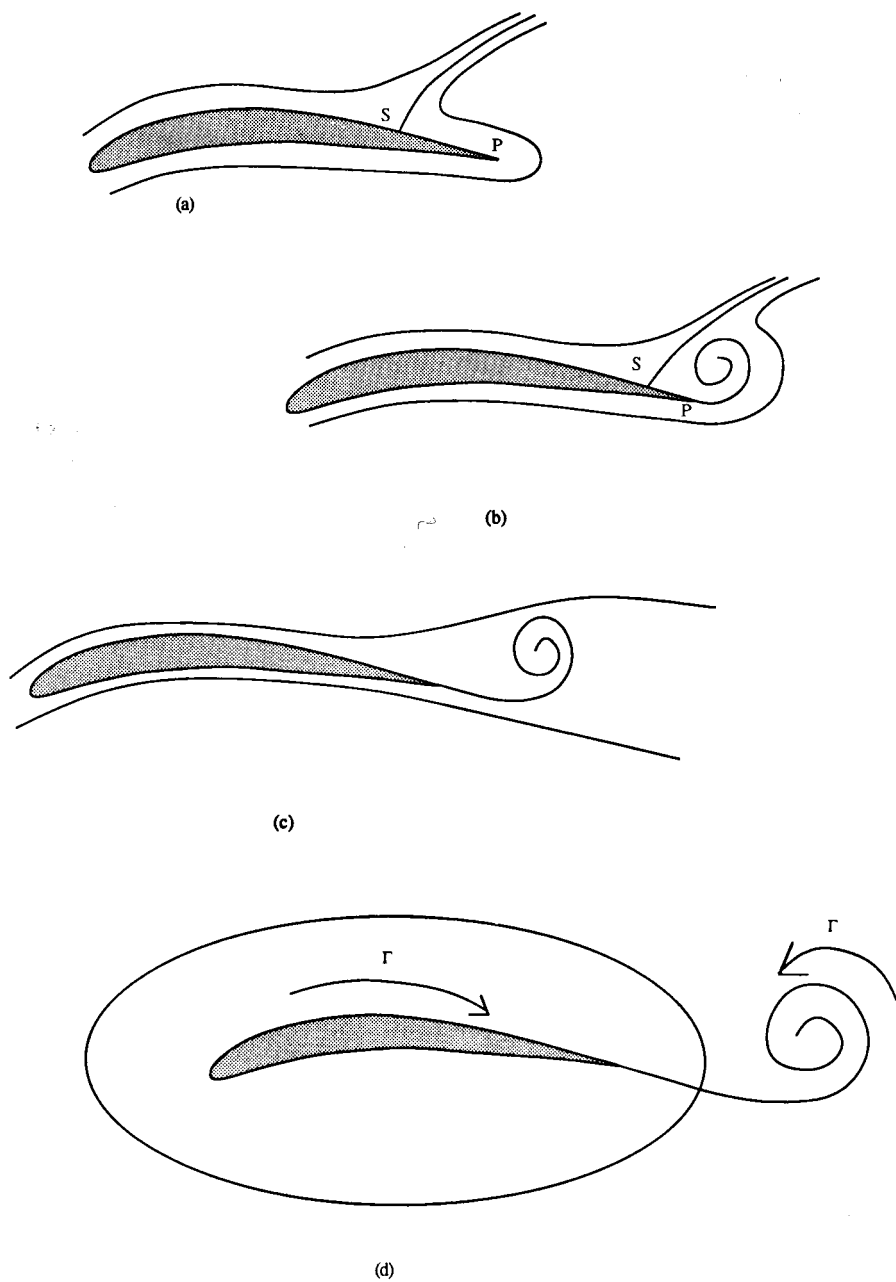
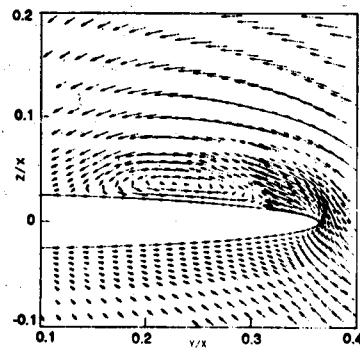


Figure 19.4.1 Mechanism behind the generation of lift on an airfoil

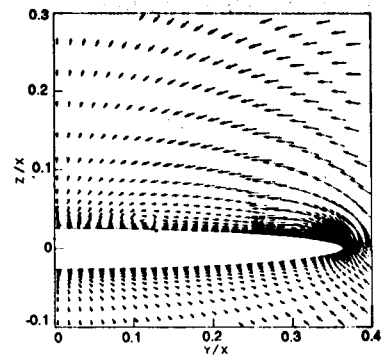
an essential, if not dominating, role in the vorticity generation at the trailing edge that feeds the eddy. Once this eddy is created the sequence of events described above proceeds in an inviscid way.

It is clear, therefore, that in the Euler computations that do not require the imposition of the Kutta condition, some mechanism has to exist that generates vorticity around the trailing edge in order to initiate the production of circulation. Remember, also, that in a real flow the physical circulation around airfoils is equal to the total amount of vorticity generated in the wall regions by viscosity (and eventually by non-uniform shocks). This vorticity feeds the downstream convected eddy.

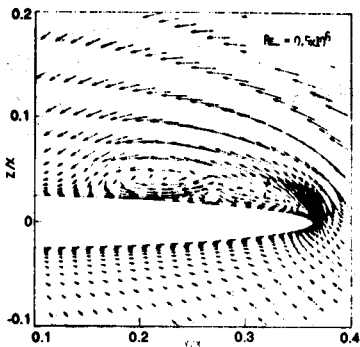
One possible mechanism can therefore be connected to the numerical dissipation present in every scheme, either from additional artificial viscosity or from the internal dissipation of the scheme needed for stability, both of which are proportional to the gradients of the flow variables and in particular of the



(a) Crossflow velocity vectors:  
coarse grid Euler



(b) Crossflow velocity vectors: fine  
grid Euler



(c) Crossflow velocity vectors:  
conical Navier - Stokes

**Figure 19.4.2** Effects of numerical dissipation on the vorticity generation in Euler flow solutions.  
(From Newsome, 1985)

velocity. This provides a mechanism for the numerical generation of vorticity (and entropy) at the scale of the mesh. With the very strong velocity gradients at the sharp edge, even very small amounts of viscosity or dissipative effects will generate local entropy layers and hence induce vorticity.

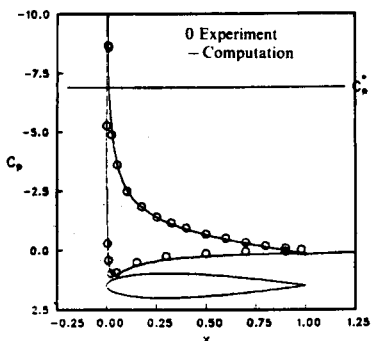
This is confirmed by various computations on coarse and fine grids (Barton and Pulliam, 1984; Newsome, 1985), which clearly show the numerical generation of vorticity or entropy layers by numerical dissipative effects. In this second reference (Newsome, 1985) an interesting test is run for a conical delta wing at supersonic Mach numbers and  $10^\circ$  incidence. This flow shows experimentally a large leading edge separation vortex and a smaller secondary viscous vortex, both of which are obtained with a Navier–Stokes computation (Figure 19.4.2c). The large separation vortex is also obtained with the Euler flow model on a coarse grid, although the smaller vortex (of viscous origin) does not appear. The coarse grid calculations are run without the imposition of a Kutta condition.

When the Euler flow is computed on a fine grid and the dissipation gradually switched off, the leading edge separation disappears from the computed solution, which is, however, a valid, converged solution of the Euler equations. When the Kutta condition is explicitly introduced in the fine grid calculations, the large local leading edge separation zone is recovered (Figure 19.4.2a, b).

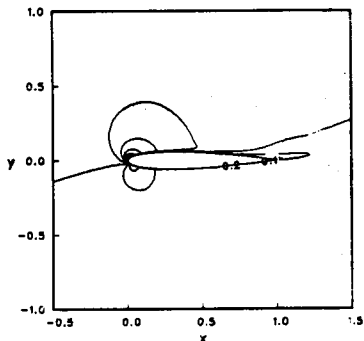
These interesting computations seem to confirm that numerical dissipation plays an essential role in the local generation of vorticity, and in addition also shows that some caution has to be exercised when interpreting numerical Euler solutions with large separated regions. Results can be obtained that are valid numerical solutions to the inviscid flow models, but that can not be considered as acceptable approximations to the limit of viscous flows for very high Reynolds numbers.

This is also shown by Barton and Pulliam (1984) for the flow along airfoils at subsonic free-stream velocities and high angles of attack. Figure 19.4.3 shows a computation of the flow along a NACA 0012 airfoil at an incident Mach number of 0.301 and  $15^\circ$  incidence, comparing a Navier–Stokes with a Euler computation on a fine mesh. The viscous, this shear layer computation gives a steady flow, fully confirmed by experimental data (Figure 19.4.3(a)), while the Euler solution is an unsteady flow with large separated vortex regions. This unsteady Euler flow is induced by the generation of vorticity due to a small normal recompression shock in the leading edge region, resulting from the strong leading edge expansion caused by the high incidence (Figure 19.4.3(b)). Although not a good approximation of the corresponding Navier–Stokes flow, it is nevertheless to be considered as a correct solution of the inviscid Euler equations.

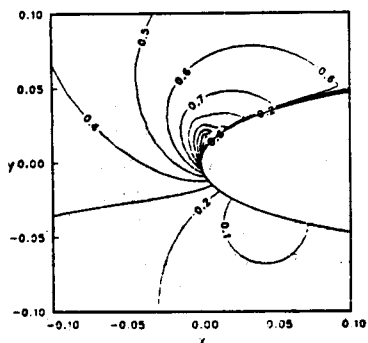
The viscous solution exhibits also a strong leading edge acceleration which remains, however, fully subsonic, so that the generated vorticity, due only to the boundary layer vorticity, is not sufficient to induce the unsteady flow pattern generally produced by large amounts of concentrated vorticity, exemplified by the Von Karman vortex street periodic flow structure.



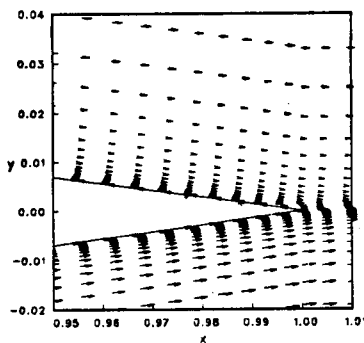
Pressure coefficient  
Comparison of thin layer Navier-Stokes  
with experimental data of McCroskey  
for  $M_\infty = 0.301$ ,  $\alpha = 15^\circ$ ,  $Re = 3.91 \times 10^6$



Mach contours  
for  $M_\infty = 0.301$ ,  $\alpha = 15^\circ$ ,  $Re = 3.91 \times 10^6$   
Thin layer Navier-Stokes

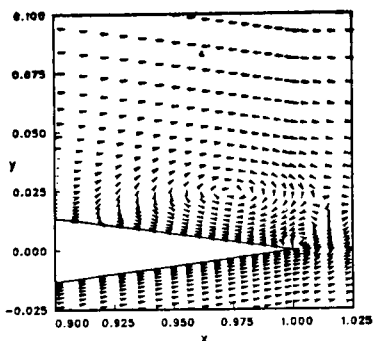


Mach contours at leading edge  
for  $M_\infty = 0.301$ ,  $\alpha = 15^\circ$ ,  $Re = 3.91 \times 10^6$   
Thin layer Navier-Stokes

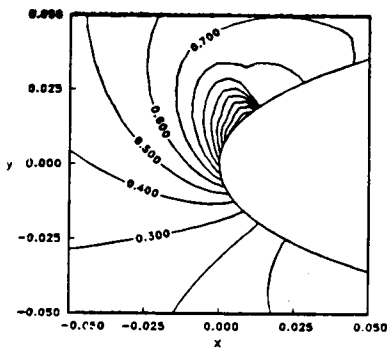


Velocity vectors at trailing edge  
showing limited extent of separation  
for  $M_\infty = 0.301$ ,  $\alpha = 15^\circ$ ,  $Re = 3.91 \times 10^6$   
Thin layer Navier-Stokes

(a) Thin shear layer Navier-Stokes calculation



Velocity vectors at trailing edge  
showing greater extent of separation  
for  $M_\infty = 0.301$ ,  $\alpha = 15^\circ$   
Euler solution, fine grid



Mach contours at leading edge  
showing strength of shock  
for  $M_\infty = 0.301$ ,  $\alpha = 15^\circ$   
Euler solution, fine grid

(b) Euler solution

Figure 19.4.3 Comparison between Euler and Navier-Stokes solutions for flow over a NACA 0012 airfoil at  $15^\circ$  incidence and 0.3 Mach number. (From Barton and Pulliam, 1984)

This suggests another mechanism that could contribute to the initial creation of an eddy at sharp edges as put forward by Rizzi (1982). In this mechanism, the large acceleration at the sharp edge leads to local supersonic flows with the subsequent creation of expansion fans, shocks and contact discontinuities, much like in the shock tube problem. The transient appearance of the shock wave creates vorticity and induces the vortex sheet surface to roll up into the eddy. Once the stagnation point is at the sharp edge, the local supersonic expansion disappears.

Note that the whole procedure described here is strongly dependent on the presence of a sharp edge. If the trailing or leading edges are rounded, then the above mechanisms do not operate and a Kutta condition is necessary to obtain lift on the smooth body. However, the position of the stagnation point at which the Kutta condition is to be imposed can only be determined by viscous considerations.

## 19.5 SUMMARY

Various methods can be adopted for the implementation of boundary conditions and any of these methods can be discretized in a variety of ways, applying various extrapolation formulas or different discretizations of the differential form of the characteristic relations.

A particular choice or combination of boundary conditions can have a considerable influence on the accuracy and even on the stability properties of the computational scheme; see, for instance, Trefethen (1983) and Foreman (1986) for examples and discussions of boundary condition influences.

It is strongly recommended to test, with any scheme, many options and combinations of implementations, by monitoring carefully the behaviour of variables at the boundaries, displaying local errors and following the conservation of variables such as total enthalpy for stationary flow problems or entropy. For instance, in test problems where exact or reference solutions are available, one should plot the detailed error evolution at the boundaries. This reveals the detailed boundary behaviour of the solution and allows the wave reflections and influence on accuracy, stability and convergence rate of the boundary treatment to be controlled.

## References

- Barton, J. T., and Pulliam, T. H. (1984). 'Airfoil computation at high angles of attack, inviscid and viscous phenomena.' *AIAA Paper 84-0524*, AIAA 22nd Aerospace Sciences Meeting.
- Batchelor, G. K. (1970). *An Introduction to Fluid Dynamics*, Cambridge: Cambridge University Press.
- Bayliss, A., and Turkel E. (1982). 'Far field boundary conditions for compressible flows.' *Journal Computational Physics*, **48**, 182-99.
- Beam, R. M., Warming, R. F., and Yee, H. C. (1981). 'Stability analysis for numerical boundary conditions and implicit difference approximations of hyperbolic equations.'

- In *Numerical Boundary Condition Procedures*, NASA CP 2201, pp. 257–82, NASA AMES Research Center.
- Chakravarthy, S. R. (1983). 'Euler equations—implicit schemes and boundary conditions.' *AIAA Journal* **21**, 699–706.
- Engquist, B., and Majda, A. (1977). 'Absorbing boundary conditions for the numerical simulation of waves.' *Mathematics of Computation*, **31**, 629–51.
- Engquist, B., and Majda, A. (1979). 'Radiation boundary conditions for acoustic and elastic wave calculations.' *Comm. Pure and Applied Mathematics*, **32**, 312–58.
- Ferm, L., Gustafsson, B. (1982). 'A downstream boundary procedure for the Euler equations.' *Computers and Fluids*, **10**, 261–276.
- Foreman, M. G. G. (1986). 'An accuracy analysis of boundary conditions for the forced shallow water equations.' *Journal Computational Physics*, **64**, 334–67.
- Giles, M. B. (1988). 'Non-reflecting boundary conditions for the Euler equations.' *Technical Report TR-88-1*, MIT Computational Fluid Dynamics Laboratory, Massachusetts Institute of Technology, USA.
- Giles, M. B. (1989). 'Non-reflecting boundary conditions for Euler equation calculations.' *AIAA Paper-89-1942*, Proc. AIAA 9th Computational Fluid Dynamics Conference, 143–152.
- Gottlieb, D., and Turkel, E. (1978). 'Boundary conditions for multistep finite difference methods for time-dependent equations.' *Journal Computational Physics*, **26**, 181–96.
- Griffin, M. D., and Anderson, J. D. (1977). 'On the application of boundary conditions to time dependent computations for quasi one dimensional fluid flows.' *Computers and Fluids*, **5**, 127–37.
- Gustafsson, B. (1975). 'The convergence rate for difference approximations to mixed initial boundary value problems.' *Mathematics of Computation*, **29**, 396–406.
- Gustafsson, B. (1982). 'The choice of numerical boundary conditions for hyperbolic systems.' *Journal of Computational Physics*, **48**, 270–283.
- Gustafsson, B., Ferm, L. (1986). 'Far field boundary conditions for steady state solutions to hyperbolic systems.' In *Nonlinear Hyperbolic Problems*. (Eds. C. Carasso, P. Raviart, D. Serre), *Lecture Notes in Mathematics*, Vol. **1270**, Springer Verlag, Berlin.
- Gustafsson, B., and Kreiss, H. O. (1979). 'Boundary conditions for time dependent problems with an artificial boundary.' *Journal Computational Physics*, **30**, 333–51.
- Gustafsson, B., Kreiss, H. O., and Sundström, A. (1972). 'Stability theory of difference approximations for mixed initial boundary value problems, II.' *Mathematics of Computation*, **26**, 649–86.
- Hedstrom, G. W. (1979). 'Non reflecting boundary conditions for non linear hyperbolic systems.' *Journal Computational Physics*, **30**, 222–37.
- Higdon, R. L. (1986). 'Initial boundary value problems for linear hyperbolic systems.' *SIAM Review*, **28**, 177–217.
- Hirsch, Ch., Verhoff, A. (1989). 'Far field numerical boundary conditions for internal and cascade flow computations.' AIAA Paper-89-1943, Proc. AIAA 9th Computational Fluid Dynamics Conference, pp. 154–168.
- Kreiss, H. O. (1968). 'Stability theory for difference approximations of mixed initial boundary value problems, I.' *Mathematics of Computation*, **22**, 703–14.
- Kreiss, H. O. (1970). 'Initial boundary value problem for hyperbolic systems.' *Comm. Pure and Applied Mathematics*, **23**, 273–98.
- Kreiss, H. O. (1974). 'Boundary conditions for hyperbolic differential equations.' *Proc. Dundee Conference on Numerical Solution of Differential Equations*, *Lecture Notes in Mathematics*, **363**, Berlin: Springer Verlag.
- Lerat, A., Sides, J., and Daru, V. (1984). 'Efficient computation of steady and unsteady transonic flows by an implicit solver.' In W. G. Habashi, (ed.), *Advances in Computational Transonics*, Pineridge Press.
- Moretti, G. (1981). 'A physical approach to the numerical treatment of boundaries in gas dynamics.' In *Numerical Boundary Condition Procedures*, NASA CP 2201, pp. 73–96, NASA AMES Research Center.

- Osher, S. (1969a). 'Systems of difference equations with general homogeneous boundary conditions.' *Trans. Am. Math. Soc.*, **137**, 177–201.
- Osher, S. (1969a). 'Stability of difference approximations of dissipative type for mixed initial-boundary value problems I.' *Mathematics of Computation*, **23**, 335–40.
- Newsome, R. W. (1985). 'A comparison of Euler and Navier–Stokes solutions for supersonic flow over a conical delta wing.' *AIAA Paper 856-0111*, AIAA 23rd Aerospace Sciences Meeting.
- Prandtl L. (1952). *Essentials of Fluid Dynamics*, London: Blackie and Sons Ltd.
- Pulliam, T. H., and Steger, J. L. (1985). 'Recent improvements in efficiency, accuracy and convergence for implicit approximate factorization algorithms.' *AIAA Paper-85-0360*, AIAA 23rd Aerospace Sciences Meeting.
- Rai, M. M., and Chaussee, D. S. (1983). 'New implicit boundary procedures: theory and applications.' *AIAA Paper 83-0123*, AIAA 21st Aerospace Sciences Meeting.
- Rizzi, A. W. (1978). 'Numerical implementation of solid-body boundary conditions for the Euler equations.' *ZAMM*, **58**, 301–4.
- Rizzi, A. (1982). 'Damped Euler equation method to compute transonic flow around wing–body combinations.' *AIAA Journal*, **20**, 1321–8.
- Rizzi, A. (1985). 'Test cases for inviscid flow field methods.' *AGARD Report AR-211*.
- Rizzi, A., and Viviand, H. (eds) (1981). Proc. GAMM Workshop on Numerical Methods for the Computation of Inviscid Transonic Flows with Shock Waves. *Notes on Numerical Fluid Dynamics*, Vol. 3, Braunschweig/Wiesbaden: Vieweg.
- Roe, P. L. (1986). 'Remote boundary conditions for unsteady multidimensional aerodynamic computations.' *ICASE Report 86–75*, NASA Langley Research Center.
- Rudy, D. H., and Strickwerda, J. C. (1980). 'A non-reflecting outflow boundary condition for subsonic Navier–Stokes calculations.' *Journal Computational Physics*, **36**, 55–70.
- Steger, J. L., Pulliam, T. H., and Chima, R. V. (1980). 'An implicit finite difference code for inviscid and viscous cascade flows.' *AIAA Paper 80-1427*, AIAA 13th Fluid and Plasma Dynamics Conference, July 1980.
- Thomas, J. L., and Salas, M. D. (1986). 'Far field boundary conditions for transonic lifting solutions to the Euler equations.' *AIAA Journal*, **24**, 1074–80.
- Thompson, K. W. (1987). 'Time dependent boundary conditions for hyperbolic systems.' *Journal Computational Physics*, **68**, 1–24.
- Trefethen, L. N. (1983). 'Group velocity interpretation of the stability theory of Gustafsson, Kreiss and Sundström.' *Journal Computational Physics*, **49**, 199–217.
- Trefethen, L. N. (1984). 'Instability of difference models for hyperbolic initial boundary value problems.' *Comm. Pure and Applied Mathematics*, **37**, 329–67.
- Trefethen, L. N. (1985). 'Stability of finite difference models containing two boundaries or interfaces.' *Mathematics of Computation*, **45**, 279–300.
- Verhoff, A. (1985). 'Modeling of computational and solid surface boundary conditions for fluid dynamics calculations.' *AIAA Paper 85-1496*, Proc. AIAA 7th Computational Fluid Dynamics Conference.
- Warming, R. F., Beam, R. M., and Yee, H. C. (1983). 'Lecture notes on the stability of difference approximations for initial boundary value problems.' *NASA Report TM-84318*.
- Wornom, S. F., and Hafez, M. M. (1984). 'A rule for selecting analytical boundary conditions for the conservative quasi-one-dimensional nozzle flow equations.' *AIAA Paper 84-0431*, AIAA 22nd Aerospace Sciences Meeting.
- Yee, H. C. (1981). 'Numerical approximations of boundary conditions with applications to inviscid gas dynamics.' *NASA Report TM-81265*.
- Yee, H. C., Beam, R. M., and Warming, R. F. (1982). 'Boundary approximation for implicit schemes for one-dimensional inviscid equations of gas dynamics.' *AIAA Journal*, **20**, 1203–11.
- Yu, N. J., Chen, H. C., Samant, A. A., and Rubbert, P. E. (1983). 'Inviscid drag calculations for transonic flows.' *AIAA Paper 83-1928*, Proc. AIAA 6th Computational Fluid Dynamics Conference, pp. 283–92.

## PROBLEMS

### Problem 19.1

Investigate the well-posedness of the system of variables  $(s, c, u)$  with regard to the acceptable combinations of boundary variables for a subsonic inlet and outlet section, following the method of Section 19.1.3. Refer also to Problem 16.19.

### Problem 19.2

Repeat Problem 19.1 for the variables  $(\rho, u, s)$  and  $(\rho, \rho u, p)$ . Refer to Problems 16.20 and 16.21.

### Problem 19.3

Apply the boundary treatment by characteristic extrapolation of Section 19.1.5 to a subsonic inlet section in a one-dimensional flow, considering that  $\rho$  and  $u$  are given as physical boundary conditions. Determine the boundary relations for  $p$  and for the conservative variables.

### Problem 19.4

Work out the boundary procedure for MacCormack's scheme applying first-order space extrapolation on the conservative variables.

Consider the four possibilities for sub/supersonic inlet/outlet sections with  $\rho$  and  $u$  fixed at a subsonic inlet and  $p$  fixed at a subsonic outlet.

Apply the relation  $\rho E = p/(\gamma - 1) + \rho u^2/2$  to obtain  $p$  at the inlet and  $\rho E$  at the outlet.

Work out this procedure for the variables  $U$  and for the variations  $\Delta U$ .

*Hint:* In the second case write at the inlet  $\Delta p/(\gamma - 1) = \Delta(\rho E) - u\Delta(\rho u) - u^2\Delta\rho/2$  where  $\Delta(\rho E)$  is extrapolated. At the outlet  $\Delta\rho$  and  $\Delta(\rho u)$  are extrapolated and  $\Delta p$  is known and generally equal to zero.

### Problem 19.5

Reproduce the boundary treatment of Example 19.1.3, based on compatibility relations and time-differenced physical boundary conditions, for imposed values of  $u$  and  $p$  at the subsonic inlet.

Find the matrices  $P_1$ ,  $P_2$  and  $P^*$ .

### Problem 19.6

Redefine the boundary procedure based on characteristic extrapolation with MacCormack's scheme, as developed in Example 19.1.1, with the non-reflecting conditions for the physical boundary values.

### Problem 19.7

Repeat Problem 19.6 with a first-order extrapolation of the conservative variables as numerical boundary conditions.

### Problem 19.8

Solve the one-dimensional stationary nozzle flow with the MacCormack scheme and first-order extrapolated boundary conditions on the conservative variables.

Consider the different cases of Problem 16.26 for the diverging nozzle and of Problem 16.27 for the converging–diverging nozzle.

Plot the errors in mass flux and the entropy and compare the results with the exact solution.

Compare with the zero-order extrapolated boundary conditions.

### Problem 19.9

Solve the one-dimensional stationary nozzle flow with the MacCormack scheme and characteristic first-order extrapolated boundary conditions, following Example 19.1.1.

Consider the different cases of Problem 16.26 for the diverging nozzle and of Problem 16.27 for the converging–diverging nozzle.

Plot the errors in mass flux and the entropy and compare the results with the exact solution.

Compare with the zero-order extrapolated boundary conditions.

### Problem 19.10

Repeat the previous problem by introducing the non-reflecting boundary conditions.

Compare also with the form (19.1.81) for the non-reflecting condition at exit.

### Problem 19.11

Develop Chakravarthy's boundary treatment for a subsonic inlet, with enthalpy  $h$  and entropy  $s$  as physical imposed variables. Work out all the matrices and equations and write them out explicitly.

### Problem 19.12

Solve the one-dimensional stationary nozzle flow with the MacCormack scheme and the boundary treatment of Example 19.1.4, with  $p$ ,  $\rho$  and  $u$  as boundary variables.

Consider the different cases of Problem 16.26 for the diverging nozzle and of Problem 16.27 for the converging–diverging nozzle.

Plot the errors in mass flux and the entropy and compare the results with the exact solution.

Compare with the zero-order extrapolated boundary conditions.

### Problem 19.13

Solve the one-dimensional stationary nozzle flow with the Beam and Warming scheme and various boundary extrapolation formulas on the conservative variables, with  $p$ ,  $u$  and  $\rho$  as boundary variables.

Consider the different cases of Problem 16.26 for the diverging nozzle and of Problem 16.27 for the converging–diverging nozzle.

Plot the errors in mass flux and the entropy and compare the results with the exact solution.

Compare with the zero-order extrapolated boundary conditions.

### Problem 19.14

Solve the one-dimensional stationary nozzle flow with the Beam and Warming scheme  $\theta = 1$ ,  $\xi = 0$  and the characteristic boundary treatment, with  $p$ ,  $u$  and  $\rho$  as boundary variables. Test different discretizations, comparing first- and second-order one-sided difference formulas.

Consider the different cases of Problem 16.26 for the diverging nozzle and of Problem 16.27 for the converging–diverging nozzle.

Plot the errors in mass flux and the entropy and compare the results with the exact solution.

Compare with the zero-order extrapolated boundary conditions.

### Problem 19.15

Solve the one-dimensional stationary nozzle flow with the Beam and Warming scheme  $\theta = 1$ ,  $\xi = 0$  and the boundary treatment of Example 19.1.4.

Consider the different cases obtained in Problems 16.26 and 16.27.

Plot the errors in mass flux and the entropy and compare the results with the exact solution.

### Problem 19.16

Solve the shock tube problem for the first case of Problem 16.25 with MacCormack's scheme, applying the compatibility relations for the numerical conditions and the non-reflective relations for the physical boundary conditions. Perform the calculations for a sufficient number of time steps until the waves reach the exit boundary.

Observe the effects of the non-reflective condition by a comparison with a one-sided discretization of the compatibility relation for the incoming characteristic.

### Problem 19.17

Define the matrix transformations for a two-dimensional flow between the characteristic variables and primitive variables. Consider the transformation of primitive variables  $Q = (u, v, p, \rho, \theta)^T$  to characteristic variables  $W = (w_1, w_2, w_3, w_4, w_5)^T$  following

**Problem 19.20**

Show from equations (19.2.28) and (19.2.29) that the normal pressure gradient can be written as

$$\frac{\partial p}{\partial n} = \rho \tilde{U} \bar{v} \cdot \frac{\partial \bar{\mathbf{1}}_n}{\partial \xi} = \rho \tilde{U} \left( u \frac{\partial \eta_x}{\partial \xi} + v \frac{\partial \eta_y}{\partial \xi} \right)$$

or as

$$\frac{\partial p}{\partial n} = - \frac{\rho \tilde{U}}{\sqrt{\eta_x^2 + \eta_y^2}} \bar{n} \cdot \frac{\partial \bar{v}}{\partial \xi} = - \frac{\rho \tilde{U}}{\sqrt{\eta_x^2 + \eta_y^2}} \left( \eta_x \frac{\partial u}{\partial \xi} + \eta_y \frac{\partial v}{\partial \xi} \right)$$

**Problem 19.21**

Consider the two-dimensional oblique shock reflection on a flat plate and discretize on a rectangular mesh defined as a cell-centred finite volume mesh, whereby no mesh points are located on the plate; refer to Figure 19.2.7.

Apply the Jameson scheme to this problem with determination of the pressure from the reflected cell method of equations (19.2.31) and (19.2.32).

Compare the convergence rates with and without residual smoothing.

**Problem 19.22**

Solve the reflected shock problem on a flat plate with the Beam and Warming scheme from a discretization with a cell vertex finite volume or, equivalently, a finite difference discretization, whereby the mesh points are on the flat plate.

Obtain the wall variables from the resolution of the difference equations at the wall by applying the interior central discretization scheme after introduction of reflected wall cells.

Compare with a discretization based on the compatibility relations at the wall for the determination of the wall variables.

**Problem 19.23**

Repeat Problem 19.22 by replacing the time integration by a fourth-order Runge–Kutta method, following Jameson's approach but keeping the same space discretization.

Compare the details of the boundary treatment with the procedure of Problem 19.21.

**Problem 19.24**

Work out in detail the discretized form for the wall pressure in the case of a curved wall as in Figure 19.2.7, following the relations (19.2.31) and (19.2.32) for a reflected wall cell.

**Problem 19.25**

Work out equation (19.2.34) when the  $\eta$  direction is not perpendicular to the wall surface, following the development of equation (19.2.32).